

# Dynamical modelling of the frailty index indicates that health reaches a tipping point near age 75

Glen Pridham<sup>1,\*</sup>, Kenneth Rockwood<sup>2</sup>, and Andrew Rutenberg<sup>1,†</sup>

<sup>1</sup>Department of Physics and Atmospheric Science, Dalhousie University, Halifax, B3H 4R2, Nova Scotia, Canada

<sup>2</sup>Division of Geriatric Medicine, Dalhousie University, Halifax, B3H 2E1, Nova Scotia, Canada

\*glen.pridham@dal.ca

†adr@dal.ca

## ABSTRACT

The frailty index (FI) serves as a useful quantitative summary of age-related health. We quantitatively modelled FI trajectories with age. We fit directly to longitudinal transitions in health attributes from normal to deficit and vice-versa. We used data from two large longitudinal studies: the Health and Retirement Study and the English Longitudinal Study of Ageing. The studies included 47592 individuals with 254357 total visits. Using damage (deficit emergence) and repair (deficit recovery) transitions we estimated changes to robustness and resilience, respectively. We find that both robustness and resilience decrease continuously with both increasing age and FI. Remarkably, these declines caused a tipping point in health near age 75, when damage and repair rates are equal. Beyond this tipping point, the ongoing loss of both robustness and resilience leads to a sharp increase in the FI and a commensurate increase in risk of mortality. This tipping point was observed in both sexes, noting that males showed higher initial robustness and resilience, and commensurately steeper decline, consistent with the sex-frailty paradox. We infer that robustness and resilience mitigate environmental stressors only up to an age of 75, beyond which health deficits will increasingly accumulate leading to death.

## Introduction

Age-related health is a dynamical process<sup>1-3</sup> characterized by complex trajectories with frequent transitions in health deficits<sup>4-6</sup>. Surprisingly, little work has been done to quantitatively analyze health trajectories<sup>7,8</sup> – which is an unaddressed question with significant implications for both public and individual health<sup>9</sup>. For example, is there a specific age at which health reaches a “tipping point”<sup>10</sup> where healthcare needs increase dramatically? Here we address the current paucity of dynamical models with a quantitative model of health trajectories as a function of both current health state and chronological age. We seek to clarify whether health deficits promote further health deficits, and whether decline is continuous or includes tipping points with advanced age or poor health.

We directly model health transitions as stochastic events. The data include 30+ health attributes, each dichotomized as either healthy (0) or deficit (1). The two possible transitions are  $0 \rightarrow 1$ , which we refer to as damage, and  $1 \rightarrow 0$ , which we referred to as repair<sup>11</sup>. Damage and repair transition rates capture changes to robustness and resilience, respectively. Robustness is defined as the ability to resist damage and resilience as the ability to repair<sup>12</sup>. Empirically, damage and repair transitions occur during transient stressor events such as acute illness<sup>6</sup>, and also prior to permanent disability<sup>5</sup>. Damage, reflecting a loss of robustness, is more likely to occur in older<sup>12</sup> and frail<sup>6</sup> individuals, and vice-versa for repair, reflecting a loss of resilience. Given that frailty is associated with age,<sup>13</sup> it has been unclear if either or both are driving the changes to resilience and robustness during aging.

We quantify health using the frailty index (FI), which is defined as the average fraction of health deficits an individual has<sup>14</sup>. Consistent with standard procedures,<sup>14,15</sup> we included 30+ health attributes from multiple domains. These included functional health, healthcare utilization, chronic disease diagnoses, signs, and symptoms. As the name suggests, the FI is sensitive to frailty, a state characterized by increased vulnerability to stressors<sup>2,13</sup>. It also efficiently summarizes overall health, particularly age-related health<sup>16</sup>. Changes to the FI occur due to transitions in health deficits, i.e. damage and repair rates, which we model as functions of both the FI and chronological age. We similarly model death hazard rates as functions of both FI and age.

Prior works suggest that the FI increases approximately exponentially with age<sup>17</sup>, leading to the damage-promotes-damage paradigm<sup>4,18</sup>. Within this paradigm, ameliorating health deficits is tantamount to anti-aging therapy – since an individual’s biologically-equivalent (biological) age depends on the average number of deficits the individual has<sup>4</sup>. Alternatively, significant damage may emerge only after underlying biological dysfunction reaches a tipping point, leading to homeostatic failure<sup>2</sup>. Identifying and characterizing such a tipping point would be particularly valuable for risk assessment, and would be a first step towards early warning signs<sup>10</sup>. Tipping points would also specify and justify the use of discrete health cutoffs, for example

age 65 is the cutoff for Medicare<sup>19</sup>, and frailty has been identified using a cutoff on the FI at 0.2,<sup>13</sup> although this value varies across studies<sup>20</sup>. Direct evidence of tipping points has been, however, notably lacking. Without a tipping point, cutoffs are arbitrary. Our model is flexible enough to permit either a tipping point or gradual decline with respect to health (the FI) and age, or both. This permits us to directly test for the existence of tipping points, and also to quantify the effect, if any, of a damage-promotes-damage paradigm.

We analyzed large-scale human longitudinal health deficit data from the Health and Retirement study (HRS) and the English Longitudinal Study of Ageing (ELSA). We fit and select joint models of damage, repair, and mortality, then simulate them to confirm they reproduce realistic population-level behaviour. The dynamical states are analyzed using the nullcline together with damage and repair rates. The nullcline (null: zero, cline: slope) is the FI-curve through age-health-state-space, along which the FI does not change. As we'll see, the expected trajectory of each individual is for their FI to move towards the nullcline. We observe that the loss of robustness and resilience with health and age is precisely fast enough to produce a tipping point near age 75. This indicates that most individuals will experience two dynamical phases during aging: a robust and resilient period of good health prior to age 75, and a period of accumulating health deficits after age 75.

## Model

We model the FI,  $f$ , as a stochastic variable satisfying

$$\frac{df}{dt} = (1 - f)D(f, t) - fR(f, t),$$

*i.e.* FI velocity = (undamaged attributes) · damage rate – (damaged attributes) · repair rate, (1)

where  $D(f, t)$  and  $R(f, t)$  are the damage and repair rates, respectively. Eq. 1 is stochastic and must be converted to an objective function to fit the data (see Methods and supplemental). Directly modelling  $D$ ,  $R$ , and the survival hazard,  $h$ , using time-to-event statistics lets us derive a log-likelihood objective function. The “mean-field” approximation of this objective function then yields Eq. 1 for the mean FI (see supplemental). This approximation becomes exact for a large number of attributes. The prefactors on the damage and repair rates, which represent the undamaged and damaged fraction of deficits, ensure that the model is not stuck at 0 and cannot exceed 1. This is in contrast to the classical exponential model<sup>17</sup> ( $df/dt = \alpha f$ ;  $\alpha > 0$ ). The specific damage and repair functions are determined during model selection.

## Data

We fit to longitudinal health and survival data. Health attributes are binary with 0 indicating normal and 1 indicating deficit (unhealthy). Health attributes are based on questionnaire data. The attribute sets used are from previous publications<sup>15,21</sup> with minor modifications as described in the supplemental. For HRS, we used waves 6-15 (2002-2020) via the RAND preprocessed files<sup>22</sup>. We included 34672 individuals with 189096 visits; median age: 66.8 (inter-quartile range: 58.7-76.0). Waves are measured every 2 years for both HRS and ELSA. For ELSA we used waves 1-8 (2002-2016)<sup>23</sup>. We included 12920 individuals with 65261 visits; median age: 67 (inter-quartile range: 60-74). ELSA survival estimates were based on end-of-life interviews, which capture only a fraction of the deaths due to a variety of response rate and fieldwork issues<sup>24</sup>. This means that we underestimate the mortality rate for ELSA because we are forced to assume that any individual without an end-of-life interview was censored instead of dying. We excluded individuals from ELSA above age 89 since those ages are top-coded, meaning that all individuals past age 89 at baseline are labelled as age 90.

## Methods

All analyses used R version 4.1.1.<sup>25</sup> We fit our model using the Broyden–Fletcher–Goldfarb–Shanno (BFGS) quasi-Newton’s method<sup>25</sup> to numerically optimize the (survival-modified) log-likelihood. The log-likelihood,  $l$ , has five terms, capturing the

four types of transitions in health together with mortality,

$$l \equiv \sum_{i=1}^N \sum_{j=1}^p \sum_{k=1}^{T-1} (1 - \delta_{ik}) \left[ \begin{array}{l} \text{sum over all individuals } (i), \text{ attributes } (j) \text{ and times } (k) \\ b_{ijk}(1 - b_{ijk-1}) \ln(1 - S_d) \quad \text{damaged } (0 \rightarrow 1) \\ + (1 - b_{ijk})b_{ijk-1} \ln(1 - S_r) \quad \text{repaired } (1 \rightarrow 0) \\ + b_{ijk}b_{ijk-1} \ln(S_r) \quad \text{did not repair } (1 \rightarrow 1) \\ + (1 - b_{ijk})(1 - b_{ijk-1}) \ln(S_d) \quad \text{did not damage } (0 \rightarrow 0) \end{array} \right] \\ + \sum_{i=1}^N \sum_{k=1}^{T-1} \left[ \ln(S(f_{ik}, f_{ik-1}, \Delta t_{ik})) + \delta_{ik} \ln(h(f_{ik}, f_{ik-1}, t_{ik})) \right], \quad \text{survived or died at time } t_{ik} \quad (2)$$

where  $N$  is the number of individuals,  $p$  the number of variables,  $T$  the number of time points.  $b_{ijk}$  is the binary health attribute of individual  $i$ , attribute  $j$  and time  $k$ .  $\delta_{ik}$  is the binary mortality indicator for individual  $i$  at time  $k$  and is 1 if the individual died at that time and 0 otherwise. The  $S$  are survival functions of the form,

$$S_d \equiv \exp\left(-\int_{t_{k-1}}^{t_k} D(f, t) dt\right) \quad (3a)$$

$$S_r \equiv \exp\left(-\int_{t_{k-1}}^{t_k} R(f, t) dt\right) \quad (3b)$$

$$S \equiv \exp\left(-\int_{t_{k-1}}^{t_k} h(f, t) dt\right) \quad (3c)$$

where  $D$ ,  $R$  and  $h$  are the damage, repair and mortality hazards, respectively. For example,  $S_d$  is the probability of an attribute ‘surviving’ damage and thus represents the (non-)transition of  $0 \rightarrow 0$ . Eq. 2 estimates the parameters of Eq. 1 in the limit of a large number of attributes. See supplemental for full details.

Prior related works using Poisson modelling suggest that transition rates should vary smoothly and approximately log-linearly with age<sup>11</sup>, and that a log-linear function of  $f$  fits well<sup>26</sup>. (Those works neglected to analyse the dynamical behaviour of the FI as a function of both age and health, which we do.) Using a log-linear model is convenient to ensure non-negative rates. We thus investigated rates with the general form

$$\ln(\Gamma) = \gamma_0 + \gamma_f f + \gamma_t t + \gamma_{ft} ft + \gamma_{f^2} f^2 \quad (4)$$

where  $\Gamma$  is a rate, including: damage,  $D$ , repair,  $R$ , or survival hazard,  $h$ . When we compare models, all rates (damage, repair and survival) have the same parametric form unless otherwise stated. The model likelihood must be solved numerically past linear order in  $t$  (Gompertz), hence we did not consider  $t^2$  (not an issue for  $f$ ). We fit directly to longitudinal binary health attribute deficit data, together with survival. During model selection we determine which of the  $\gamma_i$  are necessary to efficiently fit the data.

Missing values were uncommon. For the health attribute variables, 99.1% (HRS) and 99.8% (ELSA) of data were reported (available case), with 80.7% (HRS) and 96.2% (ELSA) of individuals having all variables measured (complete case). The least commonly measured variable that we included in the FI for HRS was difficulty climbing several flights of stairs (5.7% missing) and for ELSA was self-reported general health (0.4% missing). We fit to the available case data and simulated using the complete case data.

## Results

### 0.1 Model selection leads to a linear model in both $f$ and $t$

Model selection using either the Bayesian Information Criterion or the test log-likelihood showed that the optimal model complexity was linear dependence of both  $f$  and  $t$ , see Supplemental Figure S4. This linear model is

$$D = e^{d_0 + d_f f + d_t t} \quad (5a)$$

$$R = e^{r_0 + r_f f + r_t t} \quad (5b)$$

$$h = e^{h_0 + h_f f + h_t t} \quad (5c)$$

for damage rate  $D$ , repair rate  $R$ , and mortality (hazard) rate  $h$ . In Figure 1 we show that the linear model (blue triangles) also visually fit the mean  $f$  well, but the other statistics fit only the overall trends as compared to the ground truth (GT). The culprit for this misfit appears to be our independence assumption, since the  $p = 41$  attributes we used are strongly correlated<sup>16</sup> and thus the effective number of independent attributes should be fewer than 41. Reducing the number of independent attributes to  $p = 15$  greatly improved the visual fit for the higher order statistics (purple diamonds, see Supplemental Figure S9 for other  $p$ ). Reducing  $p$  did, however, depress the mean  $f$  at higher ages since it increases the variance and hence the hazard at larger  $f$ .<sup>27</sup>

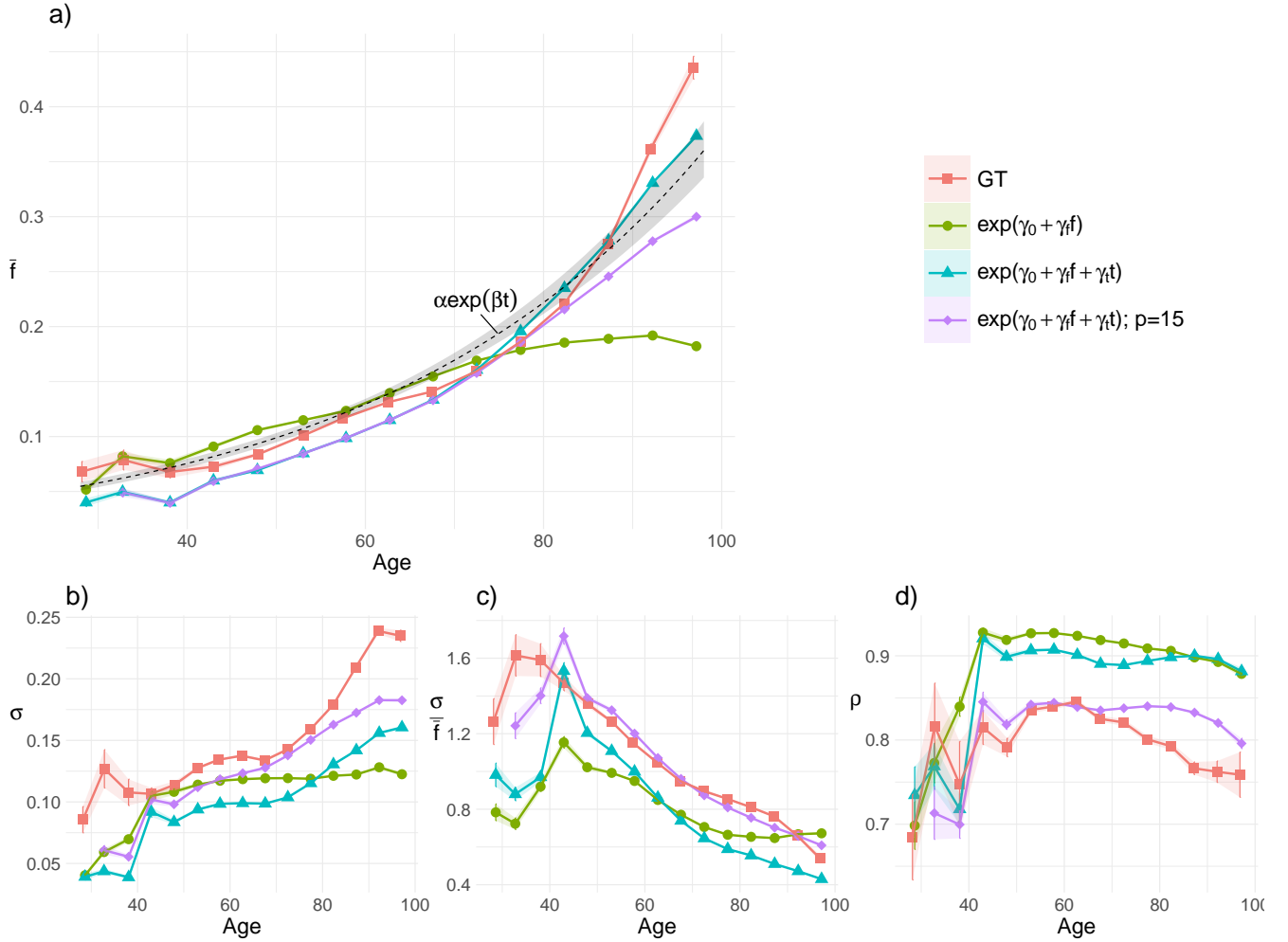


**Figure 1. FI population-level statistics** show that a linear model including  $f$  and  $t$  qualitatively recapitulates the correct FI behaviour (HRS). Simulated models versus ground truth (GT). (a) mean FI,  $\bar{f}$ , (b) FI standard deviation,  $\sigma$ , (c), coefficient of variation  $\sigma/\bar{f}$ , and (d) FI auto-correlation,  $\rho$  (lag-1). The linear model including both the FI,  $f$ , and age,  $t$ , (blue triangles) correctly captures the superlinear convexity of the mean FI (a), the complex shape of the standard deviation (b), the linearly decreasing CV past age 40 (c), and the roughly constant auto-correlation past age 40 (d). We can further improve the model fit by reducing the number of attributes from the default ( $p = 41$ ) to  $p = 15$  (purple diamonds), implying correlations between attributes are reducing the number of effective degrees of freedom<sup>16</sup>. Complete case data. Simulation was seeded with the first wave from GT. Error bars are standard errors (bootstrap, 100 repeats). Additional models in Supplemental Figure S6. For ELSA see Supplemental Figure S7.

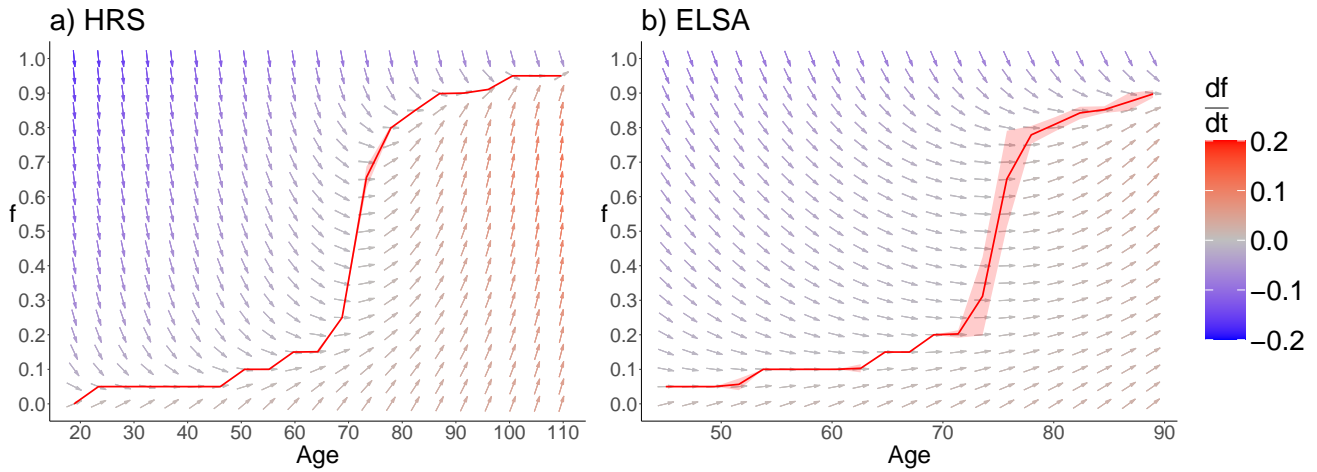


**Figure 2. FI velocity field** in terms of current health and age, for both HRS (a) and ELSA (b) data. Higher FI,  $f$ , corresponds to worse health. Arrows represent the expected direction of individual flow at each point. Blue arrows point down and will see a decrease in  $f$  over time, red arrows point up and will see an increase. The nullcline (red line) is where the  $f$  velocity is 0 and hence the expected flow only increases age (grey arrows). Observe that between ages 65-80 the nullcline increases sharply, suggesting a tipping point. Uncertainties are included in the nullcline as bands. Uncertainties in the arrows are too small to see.

## 0.2 A rapid loss of robustness and resilience with worsening health causes a tipping point near age 75

We observed that damage rate increased continuously with respect to both age and FI, indicating a loss of robustness with both age and declining health (Supplemental Figure S1). Conversely, the repair rate decreased continuously indicating a loss of resilience with both age and declining health. Damage and repair were less likely in ELSA, possibly reflecting the specific health attributes selected included more that cannot repair (e.g. “have you ever had cancer”). Death hazard rates also increased continuously with age and FI. At advanced ages and high FIs we observed hazard rates in excess of 3, indicating only a 5% chance of surviving the next year (0.25% chance of surviving until 2 year followup). Hence older individuals with high FIs will almost certainly die before followup, explaining why the FI has an empirical limit near 0.7.<sup>17</sup>

The tug-of-war between damage and repair determines the velocity field for the FI, Figure 2. By definition the velocity field is the derivative evaluated at each point in the plane,  $\frac{df}{dt}(t, f)$  using Eq. 1. An individual at any point in this plane is expected to move parallel to the local arrow. By analogy, the arrows indicates the direction of ‘wind’ pushing each individual’s FI. The nullcline, delineated by the red line, is where the FI velocity is 0. It separates regions that are expected to improve in health (blue arrows) from regions that are expected to worsen (red arrows). Points far from the nullcline typically change the fastest (vertical arrows). Remarkably, there is a sudden increase in the nullcline near age 75 in both studies, indicating a tipping point. This means, for example, that while there may be healthy individuals over age 75, they are expected to worsen commensurately to the velocity field. In Supplemental Figure S2 we show that the population density cloud is consistent with movement via the velocity field.

In Figure 3 we take a closer look at the rate of change of  $f$  with age ( $df/dt$ ) as a function of FI for different ages, as indicated by the legend. The horizontal dashed grey line is the nullcline ( $df/dt = 0$ ), which separates increasing from decreasing FI. Observe that below age 73 for HRS and age 76 for ELSA the curves never increase with  $f$ . For these younger individuals the FI velocity slows down and reverses as the FI increases, leading these individuals to stop worsening and eventually recover. In contrast, for older individuals, the FI velocity *speeds up* as the FI increases beyond very small values, causing these individuals to get even worse until a very high FI is reached, at which point imminent mortality becomes a near certainty (indicated by the greyed background, for  $f \gtrsim 0.7$ ). As we will show, a tipping point separates these young and old regimes and is caused by a rapid loss of robustness and resilience with increasing  $f$ .

The rate at which robustness and resilience are lost determines how sharply the nullcline changes and thus individual prognosis. We derive and analyse the average nullcline behavior in the supplemental, and obtain the nullcline curve

$$t^* = -\frac{\Delta_0}{\Delta_t} - \frac{\Delta_f}{\Delta_t} f^* + \frac{1}{\Delta_t} \ln\left(\frac{f^*}{1-f^*}\right), \quad (6)$$

where  $t^*$  and  $f^*$  are the times and FIs that lay on the nullcline. This nullcline curve is plotted in Figure 4, for various values

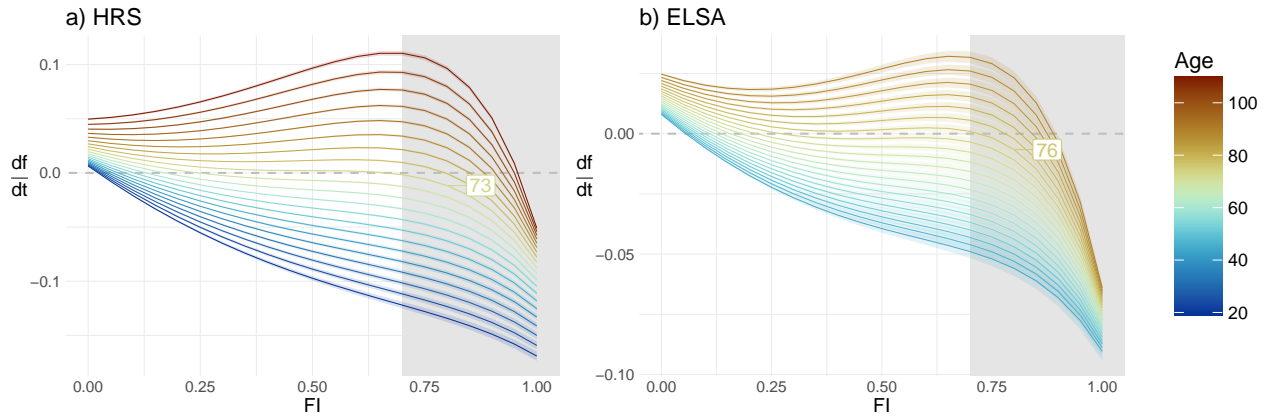


**Figure 3. FI accumulation accelerates for older individuals (ages  $\sim 75+$ ) but not for younger individuals.** Individuals will tend towards where their age-specific line (coloured lines) crosses the nullcline where the velocity  $df/dt = 0$  (grey dashed line). At young ages the velocity drops with increasing FI thus stabilizing at a low FI (blue). At older ages, 73+ for HRS and 76+ for ELSA, the velocity is constant or increasing with respect to the FI, indicating accelerating deficit accumulation (red). Eventually there are so few attributes left to damage that the FI saturates and the velocity turns negative again; but at that point mortality becomes almost certain (see Supplemental Figure S1c). FI past 0.7 was almost never observed (greyed out,  $f = 0.7$  was the 98th percentile for HRS and 99.9th for ELSA).

of  $\Delta_0 \equiv d_0 - r_0$ ,  $\Delta_t \equiv d_t - r_t$  and  $\Delta_f \equiv d_f - r_f$ . Baseline robustness and resilience,  $\Delta_0 \equiv d_0 - r_0$ , controls the position of the nullcline in time. Aging rate,  $\Delta_t \equiv d_t - r_t$ , controls the scale of the curve, with large values compressing the curve with respect to time. And finally health sensitivity,  $\Delta_f \equiv d_f - r_f$ , controls the shape of the nullcline, which is gradual for  $\Delta_f < 4$ , discontinuous for  $\Delta_f = 4$ , and bifurcates for  $\Delta_f > 4$ . The characteristic behaviour of these parameter combinations make them useful population health statistics, at least for our subsequent results.

The nullcline has a discontinuity, with  $df/dt \rightarrow \infty$  for

$$\Delta_f = \Delta_f^* \equiv 4. \quad (7)$$

Below,  $\Delta_f < 4$ , there is no discontinuity, and above,  $\Delta_f > 4$ , the discontinuity bifurcates and gradually spreads to younger ages with increasing  $\Delta_f$ . For  $\Delta_f < 4$  there is no tipping point, but instead a smooth superlinear increase. Above,  $\Delta_f > 4$ , in addition to the tipping point, there is a trap where young people who acquire a high FI are expected stay high without recovering. Remarkably, the model fits for both HRS and ELSA  $\Delta_f \equiv d_f - r_f$  yielded estimates very close to 4 ( $3.93 \pm 0.03$  for HRS and  $4.15 \pm 0.06$  for ELSA), indicating a tipping point with no bifurcation (Supplemental Figure S3). This also confirms that the loss of robustness and resilience with increasing  $f$  leads to the observed tipping point.

Our results are qualitatively identical for males and females, but the specific parameter estimates differed (Supplemental Figures S10 and S11). In particular, across studies males had lower baseline damage  $d_0$ , but were more sensitive to increasing damage with worsening health  $d_f$  and advanced age  $d_t$ ; they also experienced less of a drop in repair with worsening health  $r_f$ . They also had higher mortality rates  $h_0$  and higher risk of death with increasing FI,  $h_f$ . Overall males had better robustness and resilience at young ages but worse at older ages. This led to a lower nullcline at young ages and a higher nullcline at older ages (Supplemental Figure S12). Males also had notably higher mortality risk.

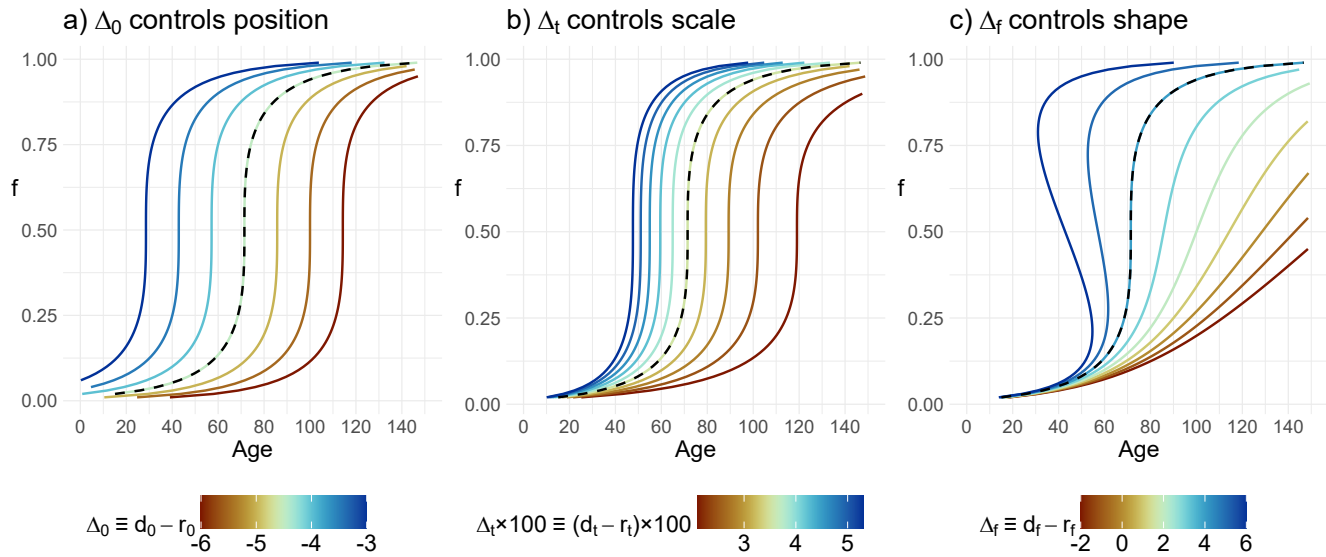


**Figure 4. The differences between parameters control the position ( $\Delta_0 = d_0 - r_0$ ), scale ( $\Delta_t = d_t - r_t$ ), and shape ( $\Delta_f = d_f - r_f$ ) of the nullcline, Eq. 6. Black dashed lines are the model fit estimates (average across studies). Notably, there is a discontinuity in the nullcline at  $\Delta_f^* = 4$ : smaller values increase gradually and larger values have a discontinuity and bifurcation (meaning there are two stable FIs: one low and one high; c). The model fit is almost exactly  $\Delta_f = 4$  leading to a nearly vertical tipping point (black dashed line in c). Individuals are expected to move towards the curve at their specific age.**

## Discussion

We dynamically modelled health trajectories due to transitions in health attributes. This permit us to directly probe robustness and damage, and resilience and repair, for health deficits. We observed that both robustness and resilience decreased continuously with increasing age and worsening health, as measured by the FI ( $f$ ). The behavior was captured in the behavior of the nullcline, which determines where average FI does not change with age. At young ages, robustness and resilience were sufficiently high that damage was uncommon and repair was swift, causing the nullcline to rest near  $f \approx 0.05$ , leading to an accordingly small FI. At older ages, both robustness and resilience were lower and the nullcline and FI instead tended towards very large values,  $f \approx 0.9$ . Mortality typically resulted before these large values could be reached. The separation between young and old was well-defined near age 75, where a singular increase of the nullcline was observed. Age 75 represents a tipping point in the aging process, after which robustness and resilience are insufficient to meet the demands of stressors.

Within our model the tipping point occurs because robustness and resilience are lost with increasing FI. Specifically, damage rate exceeds repair rate, permitting the FI to grow which further increases damage rate and decreases repair rate. This runaway process is inhibited only when the number of available undamaged attributes becomes small enough to balance the much higher probability of damage with the lower probability of repair. As a result, the nullcline increases very suddenly and only saturates just before  $f = 1$ . The effect is captured by the model by the critical value  $\Delta_f \equiv d_f - r_f = \Delta_f^* \equiv 4$ . Nevertheless, individual FI drifts relatively slowly towards the saturated nullcline, reflecting that health transitions result from relatively rare events such as illnesses<sup>6</sup> or falls that result from external stressors. This means that individuals past their tipping point age can still maintain good health before the stressors of everyday life drive them towards a high FI and ultimately death. “Healthy aging”<sup>9</sup> in these populations past age 75 is therefore predicted to require mitigation of environmental stressors, such as vaccination or removal of environmental fall hazards. Crossing the tipping point dramatically increases risk for and accumulation of health deficits if stressors are not reduced.

Our dynamical analysis provides direct evidence that frailty onset occurs at a “critical” (sudden) transition in dynamical health states<sup>2</sup>. Prior research has inferred that frailty is characterized by a state of enhanced vulnerability due to insufficient robustness and resilience to mitigate environmental demands<sup>2,13</sup>. Individuals are classified as frail if their FI exceeds  $f > 0.2$ , with higher values grading more severe cases<sup>13</sup>. We directly modelled loss of robustness and resilience and can confirm this leads to a sudden increase in vulnerability, starting at approximately  $f \approx 0.2$  (Figures 2 and S2). We observed two dynamical states at the population-level: young and old, consistent with the critical model of frailty emergence<sup>2</sup>. Indeed, FI becomes the dominant driver of health at older ages,<sup>16,28,29</sup> which is consistent with a tipping point. What’s more, we observe the changes are driven by increasing age, consistent with changes to underlying biological mechanisms<sup>2,13</sup>. Since not all individuals age at

the same rate<sup>30</sup>, we speculate that the critical transition in the nullcline could also vary between individuals.

Our dynamical analysis indicates that the tipping point emerges from gradual age-dependent changes to robustness and resilience, and that frailty increases after the tipping point result from frailty-dependent changes to robustness and resilience. Broadly speaking, age-related changes are believed to underpin frailty onset<sup>2,13</sup>, consistent with our observations. While a tipping point near age 75 appears reasonable, the exact biological mechanisms remain murky<sup>13</sup>. There are a number of significant biological changes near age 75. The proteome changes dramatically near ages 70-80.<sup>31</sup> Inflammation and the microbiome start to change around age 60,<sup>32</sup> though only inflammation is regarded as a probable biological driver of frailty<sup>13</sup>. However, some of these changes may be effects of the increase of frailty rather than direct causes of that increase. Nevertheless, our dynamical network analysis of multiple biological ages showed a dramatic change in dynamical behaviour around age 80, and indicated that the central drivers were epigenetic changes and cardiometabolic decline,<sup>28</sup> with the FI being a peripheral node (see supplemental of<sup>28</sup>). We need to further unpick the biological mechanisms underlying loss of robustness and resilience in order to better understand the subsequent gain of frailty. One path forward would be to combine our approach with deficit clustering and deep phenotyping, e.g. including genomic data<sup>33</sup>.

The “rectangular”<sup>34</sup> structure of the nullcline with a long healthy period, followed by rapid decline, delineates an optimal health trajectory<sup>34,35</sup>. While decreasing  $\Delta_f$  will improve robustness and resilience, it will also extend the decline period. An example of this would be treating a single chronic disease by glucose monitoring of diabetes, which does not prevent onset of other age-related diseases. Since there are hundreds of age-related diseases<sup>36</sup>, the impact of treating any one of these conditions will be limited without a means of treating the shared, underlying age-related mechanisms. Indeed, most Medicare recipients have 3 or more chronic conditions<sup>37</sup>. This is why contemporary frailty management seeks to directly build robustness and resilience earlier<sup>13</sup>, and could explain why the FI tends to be a better predictor of heart disease than traditional measures such as the Framingham risk score<sup>38,39</sup> (since the FI is sensitive to robustness and resilience). Interventions that target  $\Delta_f$  are sub-optimal since they act to extend the decline period. Better would be interventions that target baseline damage and repair,  $\Delta_0$ , or aging rate,  $\Delta_r$ , since either would delay the tipping point to older ages.

Stratifying by sex permitted us to explore the effects of different parameterizations since males are known to live shorter but healthier (lower FI) lives than females<sup>40</sup>. Males showed better initial robustness and resilience (smaller  $\Delta_0$ ), higher health sensitivity,  $\Delta_f$ , and faster aging rate,  $\Delta_r$ . The smaller  $\Delta_0$  delays decline whereas the higher  $\Delta_f$  and  $\Delta_r$  steepens and hastens decline, respectively. The net effect was that young males had a lower nullcline than young females, keeping their FI low. At older ages the nullclines crossed and males had a higher nullcline causing the FI to grow faster. Importantly, males also had higher mortality rates: both at baseline and with increasing FI, explaining why they died younger. These observations are consistent with known sex differences<sup>40</sup>. While the sharper decline experienced by males is desirous in terms of health-span,<sup>34,35</sup> it comes at the cost of a shorter life.

Our results suggest that the damage-promotes-damage effect<sup>4,18</sup> is driven by a moving stable nullcline rather than an instability<sup>4</sup> in the FI. Nevertheless, our parameter values indicate that robustness and resilience are both lost with increasing FI, supporting a significant degree of damage promoting further damage. In Supplemental Section S8 we show that our results can be approximated by an age-dependent instability that emerges near age  $\approx 100$ . Work in mice has shown both a saturating feedback in senescent cell count<sup>41</sup> and an instability emerging at advanced ages<sup>42</sup>, consistent with this simplified picture. The approximation also helps to explain why the average FI appears exponential at the population-level and suggests the instability picture may be a reasonable approximation<sup>4</sup>, particularly if it includes variables that could capture underlying biological changes<sup>18</sup>. In terms of trajectory forecasting, however, we predict that the FI cannot be expected to double every 15 years<sup>17</sup> – nor any other interval – as such forecasts are rooted in the exponential paradigm. Instead we predict that the FI trajectory depends on the age and current FI of the individual according to the velocity field (Figure 2).

We note a few limitations to our study. Foremost, we used an FI built entirely out of questionnaire data, which appears to only capture one of several dimensions of health<sup>16,43</sup>, although it does capture health across an impressive range of adverse health outcomes<sup>16</sup>. Some deficits cannot repair by definition and hence our interpretation of resilience is subject to the caveat that we have included these variables – which are typically included in the FI. We are furthermore agnostic to what constitutes repair, which could represent resolution of a deficit like a fall injury, or adapted behaviour by an individual to negate the effects of a deficit, like adding a grab bar to make a bathtub more accessible. Stressor events that do not cause deficits, such as falls without injuries, are invisible to our analysis. The timescale over which we observe damage and repair events is also an important caveat. The data are sampled every 2 years, and we therefore cannot comment on robustness and resilience on significantly shorter timescales (e.g. with respect to acute diseases such as the flu).

The model parameters are highly interpretable since they directly affect damage, repair and hazard rates. The differences between parameters also appear to be highly interpretable:  $\Delta_0$  delays decline,  $\Delta_r$  scales age, and  $\Delta_f$  controls the sharpness of decline. This makes either the parameters or their differences a tool for analyzing population health, and interpreting the effects of interventions or associations with desirable aging trajectories, including identifying drivers of frailty. The discontinuity in the age range of 70-80 suggests this is the key discriminating age range for assessing the effectiveness of interventions that



mitigate or delay decline. Future research should consider: (i) fitting the model to sub-populations of interest (e.g. treatment vs control), (ii) modifying the model to permit covariates to identify associations (such as in  $\Delta_0$  and  $\Delta_t$ ), and (iii) completely individualizing the model fits. It is interesting to consider how these parameters could help to parse known associations with the FI, such as social vulnerability<sup>44</sup> and physical exercise<sup>7</sup>.

Age-related health includes complex trajectories with individuals experiencing many transitions in health attributes. These transitions appear to capture the effects of stochastic stressor events such as illnesses or falls. Trajectories can be quantitatively modelled using damage and repair of health attributes that capture robustness and resilience, respectively. Such quantitative models can be analyzed to infer general behaviour of the population of interest, and to identify underlying drivers. This enhances our knowledge of what aging health trajectories look like. Here we provide an analysis of natural, *in situ*, aging of human populations. We find that natural aging dynamics are non-trivial and include a tipping point near age 75 where robustness and resilience become insufficient and after which individuals tend towards worse health over time, marking an end to a robust and resilient youthful period.

## **Acknowledgments**

ADR thanks the Natural Sciences and Engineering Research Council of Canada (NSERC) for operating Grant RGPIN-2019-05888. The HRS (Health and Retirement Study) is sponsored by the National Institute on Aging (grant number NIA U01AG009740) and is conducted by the University of Michigan. ELSA is funded by the National Institute on Aging (R01AG017644), and by UK Government Departments coordinated by the National Institute for Health and Care Research (NIHR).

## **Author contributions statement**

ADR and KR supervised. ADR conceived the project and contributed to analysis. GP did the primary analysis and initial draft. All authors reviewed the manuscript.

## **Disclosures**

None.

## References

1. Rattan, S. I. S. Healthy ageing, but what is health? *Biogerontology* **14**, 673–677, DOI: [10.1007/s10522-013-9442-7](https://doi.org/10.1007/s10522-013-9442-7) (2013).
2. Fried, L. P. *et al.* The physical frailty syndrome as a transition from homeostatic symphony to cacophony. *Nat. Aging* **1**, 36–46, DOI: [10.1038/s43587-020-00017-z](https://doi.org/10.1038/s43587-020-00017-z) (2021).
3. Cohen, A. A. *et al.* A complex systems approach to aging biology. *Nat. Aging* **2**, 580–591, DOI: [10.1038/s43587-022-00252-6](https://doi.org/10.1038/s43587-022-00252-6) (2022).
4. Mitnitski, A. & Rockwood, K. Aging as a process of deficit accumulation: its utility and origin. *Interdiscip. Top. Gerontol.* **40**, 85–98, DOI: [10.1159/000364933](https://doi.org/10.1159/000364933) (2015).
5. Manini, T. Development of physical disability in older adults. *Curr. Aging Sci.* **4**, 184–191, DOI: [10.2174/1874609811104030184](https://doi.org/10.2174/1874609811104030184) (2011).
6. Lees, C. *et al.* Frailty hinders recovery from influenza and acute respiratory illness in older adults. *J. Infect. Dis.* **222**, 428–437, DOI: [10.1093/infdis/jiaa092](https://doi.org/10.1093/infdis/jiaa092) (2020).
7. Howlett, S. E., Rutenberg, A. D. & Rockwood, K. The degree of frailty as a translational measure of health in aging. *Nat. Aging* **1**, 651–665, DOI: [10.1038/s43587-021-00099-3](https://doi.org/10.1038/s43587-021-00099-3) (2021).
8. Zhang, W. *et al.* The correlation between frailty trajectories and adverse outcomes in older patients: A systematic review. *Arch. Gerontol. Geriatr.* **128**, 105622, DOI: [10.1016/j.archger.2024.105622](https://doi.org/10.1016/j.archger.2024.105622) (2025).
9. Michel, J.-P. & Sadana, R. “healthy aging” concepts and measures. *J. Am. Med. Dir. Assoc.* **18**, 460–464, DOI: [10.1016/j.jamda.2017.03.008](https://doi.org/10.1016/j.jamda.2017.03.008) (2017).
10. Scheffer, M. *et al.* Anticipating critical transitions. *Science* **338**, 344–348, DOI: [10.1126/science.1225244](https://doi.org/10.1126/science.1225244) (2012).
11. Farrell, S., Kane, A. E., Bisset, E., Howlett, S. E. & Rutenberg, A. D. Measurements of damage and repair of binary health attributes in aging mice and humans reveal that robustness and resilience decrease with age, operate over broad timescales, and are affected differently by interventions. *Elife* **11**, e77632, DOI: [10.7554/eLife.77632](https://doi.org/10.7554/eLife.77632) (2022).
12. Ukraintseva, S., Yashin, A. I. & Arbee, K. G. Resilience versus robustness in aging. *J. Gerontol. A Biol. Sci. Med. Sci.* **71**, 1533–1534, DOI: [10.1093/gerona/glw083](https://doi.org/10.1093/gerona/glw083) (2016).
13. Kim, D. H. & Rockwood, K. Frailty in older adults. *N. Engl. J. Med.* **391**, 538–548, DOI: [10.1056/NEJMra2301292](https://doi.org/10.1056/NEJMra2301292) (2024).
14. Searle, S. D., Mitnitski, A., Gahbauer, E. A., Gill, T. M. & Rockwood, K. A standard procedure for creating a frailty index. *BMC Geriatr.* **8**, 24, DOI: [10.1186/1471-2318-8-24](https://doi.org/10.1186/1471-2318-8-24) (2008).
15. Theou, O., Haviva, C., Wallace, L., Searle, S. D. & Rockwood, K. How to construct a frailty index from an existing dataset in 10 steps. *Age Ageing* **52**, 1–7, DOI: [10.1093/ageing/afad221](https://doi.org/10.1093/ageing/afad221) (2023).
16. Pridham, G., Rockwood, K. & Rutenberg, A. Efficient representations of binarized health deficit data: the frailty index and beyond. *Geroscience* **45**, 1687–1711, DOI: [10.1007/s11357-022-00723-z](https://doi.org/10.1007/s11357-022-00723-z) (2023).
17. Mitnitski, A. & Rockwood, K. The rate of aging: the rate of deficit accumulation does not change over the adult life span. *Biogerontology* **17**, 199–204, DOI: [10.1007/s10522-015-9583-y](https://doi.org/10.1007/s10522-015-9583-y) (2016).
18. Taneja, S., Mitnitski, A. B., Rockwood, K. & Rutenberg, A. D. Dynamical network model for age-related health deficits and mortality. *Phys Rev E* **93**, 022309, DOI: [10.1103/PhysRevE.93.022309](https://doi.org/10.1103/PhysRevE.93.022309) (2016).
19. Aggarwal, R., Yeh, R. W., Dahabreh, I. J., Robertson, S. E. & Wadhwa, R. K. Medicare eligibility and healthcare access, affordability, and financial strain for low- and higher-income adults in the united states: A regression discontinuity analysis. *PLoS Med.* **19**, e1004083, DOI: [10.1371/journal.pmed.1004083](https://doi.org/10.1371/journal.pmed.1004083) (2022).
20. Gordon, E. H., Reid, N., Khetani, I. S. & Hubbard, R. E. How frail is frail? a systematic scoping review and synthesis of high impact studies. *BMC Geriatr.* **21**, 719, DOI: [10.1186/s12877-021-02671-3](https://doi.org/10.1186/s12877-021-02671-3) (2021).
21. Rogers, N. T., Steptoe, A. & Cadar, D. Frailty is an independent predictor of incident dementia: Evidence from the English Longitudinal Study of Ageing. *Sci. Rep.* **7**, 15746, DOI: [10.1038/s41598-017-16104-y](https://doi.org/10.1038/s41598-017-16104-y) (2017).
22. Health and retirement study, RAND HRS longitudinal file 2020 (v2). University of Michigan with funding from the National Institute on Aging, Ann Arbor, MI (2024).
23. Banks, J., Batty, G. David, Breedvelt, J., Coughlin, K., Crawford, R., Marmot, M., Nazroo, J., Oldfield, Z., Steel, N., Steptoe, A., Wood, M., Zaninotto, P. English longitudinal study of ageing (ELSA). UK Data Service, DOI: [10.5255/UKDA-SN-5050-27](https://doi.org/10.5255/UKDA-SN-5050-27) (2024).

24. NatCen Social Research. *English Longitudinal Study of Ageing (ELSA) Wave 2 to Wave 6 User Guide to the End of Life interview datasets*. NatCen (2015).
25. R Core Team. *R: A language and environment for statistical computing* (2021).
26. Mitnitski, A., Bao, L. & Rockwood, K. Going from bad to worse: a stochastic model of transitions in deficit accumulation, in relation to mortality. *Mech. Ageing Dev.* **127**, 490–493, DOI: [10.1016/j.mad.2006.01.007](https://doi.org/10.1016/j.mad.2006.01.007) (2006).
27. Pridham, G., Tennankore, K. K., Rockwood, K., Worthen, G. & Rutenberg, A. D. Systems-level health of patients living with end-stage kidney disease using standard lab values. *arXiv [q-bio.QM]* (2024). [2405.20523](https://arxiv.org/abs/2405.20523).
28. Pridham, G. & Rutenberg, A. D. Dynamical network stability analysis of multiple biological ages provides a framework for understanding the aging process. *J. Gerontol. A Biol. Sci. Med. Sci.* DOI: [10.1093/geron/glae021](https://doi.org/10.1093/geron/glae021) (2024).
29. Farrell, S. G., Mitnitski, A. B., Rockwood, K. & Rutenberg, A. D. Network model of human aging: Frailty limits and information measures. *Phys Rev E* **94**, 052409, DOI: [10.1103/PhysRevE.94.052409](https://doi.org/10.1103/PhysRevE.94.052409) (2016).
30. Jylhävä, J., Pedersen, N. L. & Hägg, S. Biological age predictors. *EBioMedicine* **21**, 29–36, DOI: [10.1016/j.ebiom.2017.03.046](https://doi.org/10.1016/j.ebiom.2017.03.046) (2017).
31. Lehallier, B. *et al.* Undulating changes in human plasma proteome profiles across the lifespan. *Nat. Med.* **25**, 1843–1850, DOI: [10.1038/s41591-019-0673-2](https://doi.org/10.1038/s41591-019-0673-2) (2019).
32. Shen, X. *et al.* Nonlinear dynamics of multi-omics profiles during human aging. *Nat. Aging* 1–16, DOI: [10.1038/s43587-024-00692-2](https://doi.org/10.1038/s43587-024-00692-2) (2024).
33. Foote, I. F. *et al.* Uncovering the multivariate genetic architecture of frailty with genomic structural equation modelling. *medRxiv* 2024.07.24.24310923, DOI: [10.1101/2024.07.24.24310923](https://doi.org/10.1101/2024.07.24.24310923) (2024).
34. Seals, D. R., Justice, J. N. & LaRocca, T. J. Physiological geroscience: targeting function to increase healthspan and achieve optimal longevity. *J. Physiol.* **594**, 2001–2024, DOI: [10.1113/jphysiol.2014.282665](https://doi.org/10.1113/jphysiol.2014.282665) (2016).
35. Kennedy, D. Longevity, quality, and the one-hoss shay. *Science* **305**, 1369, DOI: [10.1126/science.305.5689.1369](https://doi.org/10.1126/science.305.5689.1369) (2004).
36. Katzir, I. *et al.* Senescent cells and the incidence of age-related diseases. *Aging Cell* **20**, e13314, DOI: [10.1111/accel.13314](https://doi.org/10.1111/accel.13314) (2021).
37. Fabbri, E. *et al.* Aging and multimorbidity: New tasks, priorities, and frontiers for integrated gerontological and clinical research. *J. Am. Med. Dir. Assoc.* **16**, 640–647, DOI: [10.1016/j.jamda.2015.03.013](https://doi.org/10.1016/j.jamda.2015.03.013) (2015).
38. Farooqi, M. A. M., Gerstein, H., Yusuf, S. & Leong, D. P. Accumulation of deficits as a key risk factor for cardiovascular morbidity and mortality: A pooled analysis of 154 000 individuals. *J. Am. Hear. Assoc.* **9**, e014686, DOI: [10.1161/JAHA.119.014686](https://doi.org/10.1161/JAHA.119.014686) (2020).
39. Wallace, L. M. K. *et al.* Accumulation of non-traditional risk factors for coronary heart disease is associated with incident coronary heart disease hospitalization and death. *PLoS One* **9**, e90475, DOI: [10.1371/journal.pone.0090475](https://doi.org/10.1371/journal.pone.0090475) (2014).
40. Hubbard, R. E. Sex differences in frailty. *Interdiscip Top Gerontol Geriatr* **41**, 41–53, DOI: [10.1159/000381161](https://doi.org/10.1159/000381161) (2015).
41. Karin, O., Agrawal, A., Porat, Z., Krizhanovsky, V. & Alon, U. Senescent cell turnover slows with age providing an explanation for the Gompertz law. *Nat. Commun.* **10**, 5495, DOI: [10.1038/s41467-019-13192-4](https://doi.org/10.1038/s41467-019-13192-4) (2019).
42. Avchaciov, K. *et al.* Unsupervised learning of aging principles from longitudinal data. *Nat. Commun.* **13**, 6529, DOI: [10.1038/s41467-022-34051-9](https://doi.org/10.1038/s41467-022-34051-9) (2022).
43. Widagdo, I. S., Pratt, N., Russell, M. & Roughead, E. E. Construct validity of four frailty measures in an older Australian population: A Rasch analysis. *J Frailty Aging* **5**, 78–81, DOI: [10.14283/jfa.2016.83](https://doi.org/10.14283/jfa.2016.83) (2016).
44. Ayeni, A., Sharples, A. & Hewson, D. The association between social vulnerability and frailty in community dwelling older people: A systematic review. *Geriatr. (Basel)* **7**, 104, DOI: [10.3390/geriatrics7050104](https://doi.org/10.3390/geriatrics7050104) (2022).
45. Wickham, H. *ggplot2: Elegant graphics for data analysis* (2016).
46. Pridham, G. & Rutenberg, A. D. Network dynamical stability analysis reveals key “mallostatic” natural variables that erode homeostasis and drive age-related decline of health. *Sci. Rep.* **13**, 1–12, DOI: [10.1038/s41598-023-49129-7](https://doi.org/10.1038/s41598-023-49129-7) (2023).
47. Yang, Y. *et al.* Damage dynamics and the role of chance in the timing of E. coli cell death. *Nat. Commun.* **14**, 2209, DOI: [10.1038/s41467-023-37930-x](https://doi.org/10.1038/s41467-023-37930-x) (2023).
48. Bender, R., Augustin, T. & Blettner, M. Generating survival times to simulate Cox proportional hazards models. *Stat. Med.* **24**, 1713–1723, DOI: [10.1002/sim.2059](https://doi.org/10.1002/sim.2059) (2005).
49. Robert, C. & Casella, G. *Introducing Monte Carlo Methods with R* (Springer New York, 2010).

## S1 Supplemental information for: dynamical modelling of the frailty index indicates that health reaches a tipping point near age 75

This supplemental includes additional results and supporting evidence for the main text. We begin with additional results that were not included in the main text for want of space in Section S1.1. We provide additional details on the specific FI variables used in Section S1.2. Model selection is performed in Section S1.3, where we show that the model linear in both FI and age is the best choice. We then compare population-level statistics for both ELSA and HRS using additional models in Section S1.4 (compared to Figure 1). This includes the survival curves using a proportional hazard assumption (i.e.  $\ln(h) \propto f$ ).

In Section S1.5 we tune the number of health attributes, which shows that reducing the effective number of health attributes improves the fit to higher-order population-level statistics (variance, coefficient of variation and auto-correlation).

We then consider sex effects by fitting separately to males and females in Section S1.6. While the main results are the same, the specific parameterizations of males and females are different, capturing known differences between males and females<sup>40</sup> (males tend to live shorter but healthier lives: the sex-frailty paradox).

Finally we disclose the mathematical derivations underlying our results. This begins with an analysis of the model nullcline in Section S1.7. Next we derive the objective function, the survival-modified log-likelihood, in Section S1.8. We include the gradient for efficient optimization, and a short proof of self-consistency between the log-likelihood formalism and Eq. 1. We derive an approximation of our model in Section S1.9 which makes it easier to compare our results to other models. Lastly, we provide the math needed to simulate our results in Section S1.10.

### S1.1 Additional results

The model estimates for damage, repair and death hazard rates are plotted in Figure S5. Observe that damage and death rates increased continuously with age and increasing FI, whereas repair rates decreased. Increasing damage rate indicates a loss of robustness whereas decreasing repair rate indicates a loss of resilience.

The velocity field,  $df/dt$ , is based on model predictions, and allows us to inquire what parts of the velocity field are actually occupied by observed individuals. The population densities are added as contours to the velocity fields in Figure S6. As we can see, the population is heavily concentrated at low FIs and intermediate ages. Despite this, it is visually plausible that the population is being pushed by the velocity field in analogy to a cloud in the wind (big arrows). At the same time, stochastic effects serve to scatter the population, against the velocity field — while mortality effects prune the population at larger FIs.

The estimated fit parameters for 100 bootstrap replicates are presented in Figure S7. Observe that in both studies  $\Delta_f \approx 4$ , which is precisely the value for which there is a vertical tipping point in the nullcline.

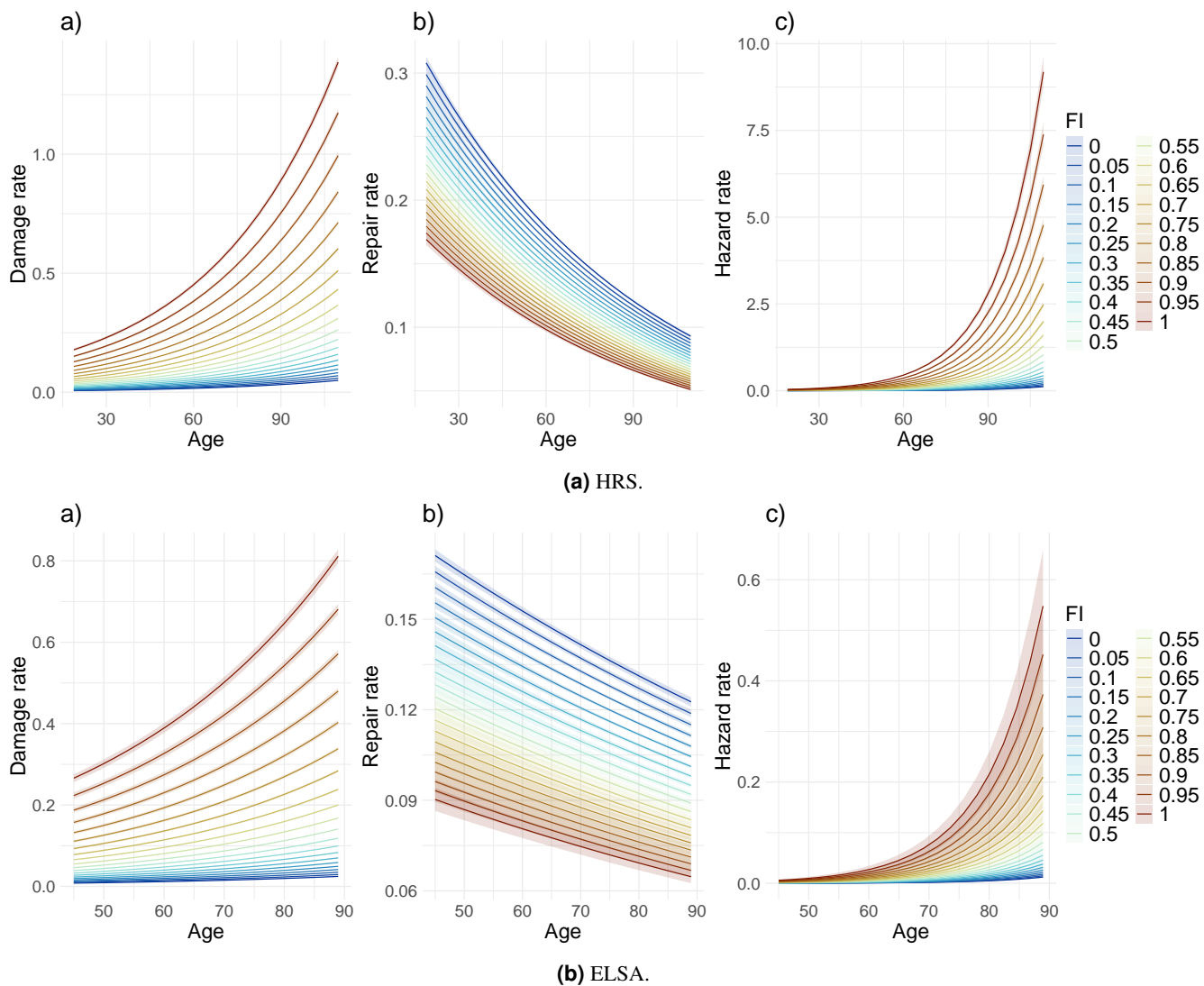


**Figure S5. Robustness and resilience decrease continuously with age and FI, and death hazard increases.** ELSA survival hazard is low compared to HRS because only a fraction of deaths are recorded in the end-of-life files<sup>24</sup>. Nevertheless, the age and FI dependence for survival is similar for both studies. Parameter estimates with standard errors (100 repeat bootstrap).

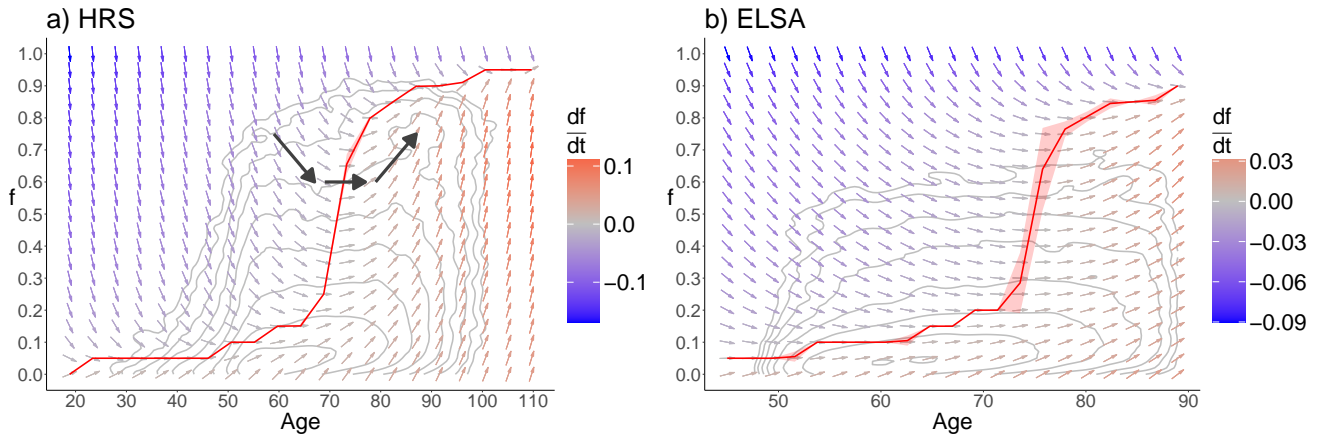


**Figure S6. FI velocity field** in terms of current health and age. Higher FI,  $f$ , corresponds to worse health. Small arrows represent the expected flow of individuals at each point. Blue arrows will see a decrease in  $f$  over time, red arrows will see an increase. The grey lines are population density contours (binned on a  $\log_2$ -scale). The population appears to follow the field lines in (a) as indicated by the big arrows. The nullcline (red line) is where the velocity is 0 and hence the expected flow is no change to  $f$ . Uncertainties in the arrows are too small to see.

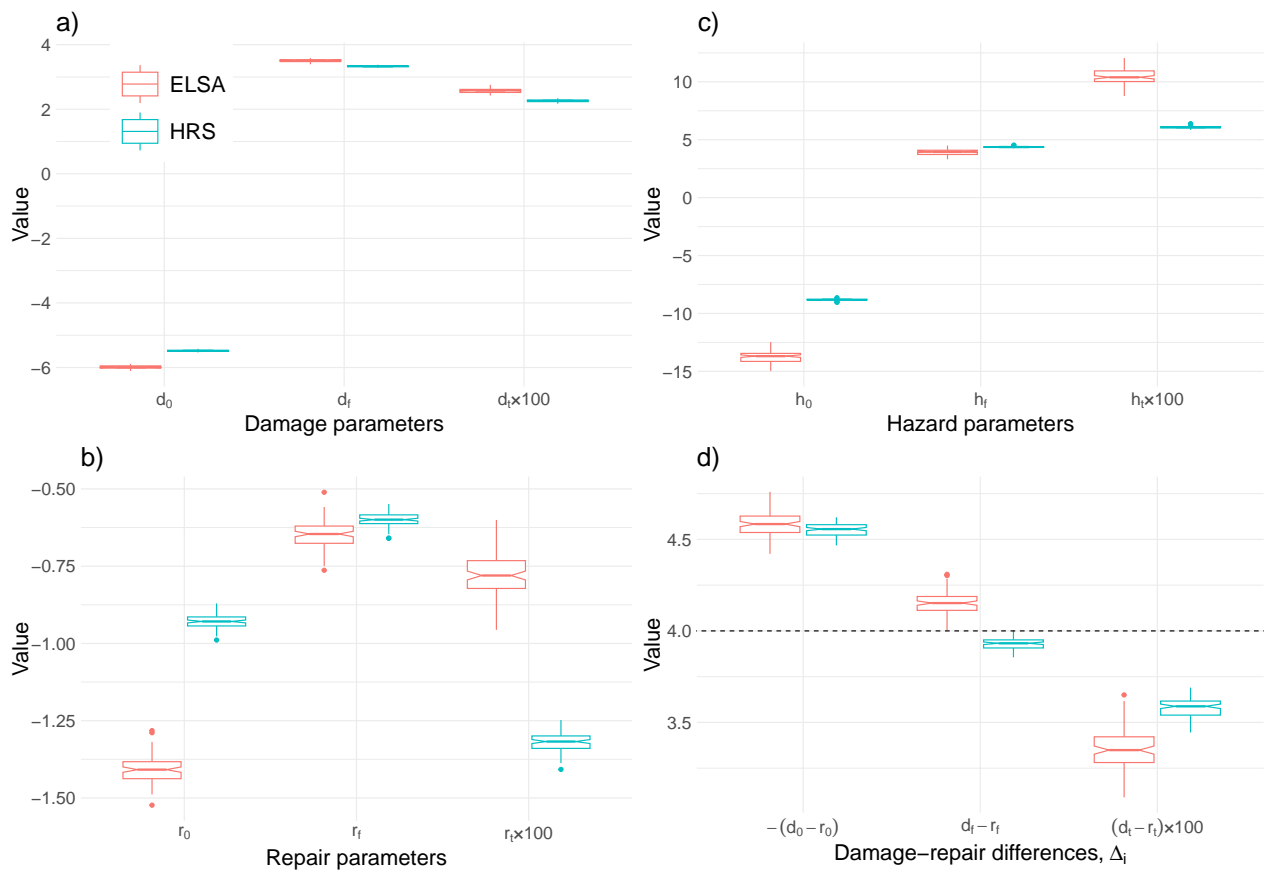


**Figure S7. Parameter estimates.** Parameter estimates from ELSA (left, red) and HRS (blue, right) are mostly comparable (a-c) – particularly the damage-repair differences in (d) that control the nullcline position, scale, and shape. The shape parameter  $\Delta_f \equiv d_f - r_f$  is very close to 4, where a discontinuity in the nullcline appears (see Section S1.7 details). Changes to robustness appear to dominate, with  $|d_f| > |r_f|$  and  $|d_f| > |r_f|$  (a and b). Bar is median, notch is approximate 95% CI for median, box is interquartile range (IQR), whiskers are  $1.5 \times \text{IQR}$  or furthest datum<sup>45</sup> from 100 bootstrap replicates.

## **S1.2 FI variables**

We seek to model a realistic FI and hence followed standard rules. For the FI we included 30+ variables from multiple domains<sup>14</sup>. We used the HRS rand FI developed elsewhere by Theou *et al.*<sup>15</sup>. We excluded one variable: number of doctor visits in previous 2 years, since it was not obvious how to binarize in a sample-independent manner. The specific variables used are reported in Table [S1](#).

For ELSA, our list of FI variables is based on previous work by Rogers *et al.*<sup>21</sup>. We modified their list by excluding 8 depressive symptoms for sake of convenience. In an effort to compensate for losing these cognitive variables, we extended their list to include Parkinson's, Alzheimer's and dementia diagnoses. The specific list is given in Table [S2](#).

**Table S1.** HRS FI variables used

Code	Description	Encoding	
1	armsa	Difficulty reaching/extending arms up	0: no, 1: yes/any
2	arthre	Ever diagnosed with arthritis	0: no, 1: yes
3	batha	Difficulty bathing or showerng	0: no, 1: yes/any
4	bathh	Gets help bathing, showerng	0: no, 1: yes
5	beda	Difficulty getting in/out of bed	0: no, 1: yes/any
6	bede	Uses equipment to get in/out of bed	0: no, 1: yes
7	bedh	Gets help getting in/out of bed	0: no, 1: yes
8	cancre	Ever diagnosed with cancer	0: no, 1: yes
9	chaira	Difficulty getting up from chair	0: no, 1: yes/any
10	clim1a	Difficulty climbing one stair flight	0: no, 1: yes/any
11	climsa	Difficulty climbing several stair flight	0: no, 1: yes/any
12	diabe	Ever diagnosed with diabetes	0: no, 1: yes
13	dimea	Difficulty picking up a dime	0: no, 1: yes/any
14	dressa	Difficulty dressing	0: no, 1: yes/any
15	dressh	Gets help dressing	0: no, 1: yes
16	eata	Difficulty eating	0: no, 1: yes/any
17	eath	Gets help eating	0: no, 1: yes
18	hearte	Ever diagnosed with heart problems	0: no, 1: yes
19	hibpe	Ever diagnosed with high blood pressure	0: no, 1: yes
20	homcar	Received home health care within previous 2 years	0: no, 1: yes
21	hosp	Had a hospital stay within previous 2 years	0: no, 1: yes
22	lifta	Difficulty lifting/carrying 10lbs	0: no, 1: yes/any
23	lunge	Ever diagnosed with lung disease	0: no, 1: yes
24	moneya	Difficulty managing money	0: no, 1: yes/any
25	nhmliv	Living in nursing home at time of interview	0: no, 1: yes
26	nrshom	Had a nursing home stay within previous 2 years	0: no, 1: yes
27	outpt	Had outpatient surgery within previous 2 years	0: no, 1: yes
28	phonea	Difficulty using the telephone	0: no, 1: yes/any
29	pusha	Difficulty pushing/pulling a large object	0: no, 1: yes/any
30	shlt	Self-reported health	0: excellent-good, 1: fair-poor
31	shopa	Difficulty shopping for groceries	0: no, 1: yes/any
32	spcfac	Visited a specialized health facility within previous 2 years	0: no, 1: yes
33	stoopa	Difficulty stooping/kneeling/crouching	0: no, 1: yes/any
34	stroke	Ever diagnosed with a stroke	0: no, 1: yes
35	toilta	Difficulty using the toilet	0: no, 1: yes/any
36	toilth	Gets help using the toilet	0: no, 1: yes
37	walk1a	Difficulty walking one block	0: no, 1: yes/any
38	walkra	Difficulty walking across rooms	0: no, 1: yes/any
39	walkre	Needs equipment to walk across rooms	0: no, 1: yes
40	walkrh	Gets help walking across rooms	0: no, 1: yes
41	walksa	Difficulty walking several blocks	0: no, 1: yes/any



**Table S2.** ELSA FI variables used

	Description	Encoding
1	Difficulty walking 100 yards	0: no, 1: yes
2	Difficulty sitting for about two hours	0: no, 1: yes
3	Difficulty getting up from a chair after sitting for long periods	0: no, 1: yes
4	Difficulty climbing several flights of stairs without resting	0: no, 1: yes
5	Difficulty climbing one flight of stairs without resting	0: no, 1: yes
6	Difficulty stooping kneeling or crouching	0: no, 1: yes
7	Difficulty reaching or extending arms above shoulder level	0: no, 1: yes
8	Difficulty pulling pushing large objects like a living room chair	0: no, 1: yes
9	Difficulty lifting carrying over 10 lbs like a heavy bag of groceries	0: no, 1: yes
10	Difficulty picking up a 5p coin from a table	0: no, 1: yes
11	Difficulty dressing including putting on shoes and socks	0: no, 1: yes
12	Difficulty walking across a room	0: no, 1: yes
13	Difficulty bathing or showering	0: no, 1: yes
14	Difficulty eating such as cutting up your food	0: no, 1: yes
15	Difficulty getting in or out of bed	0: no, 1: yes
16	Difficulty using the toilet including getting up or down	0: no, 1: yes
17	Difficulty using a map to get around in a strange place	0: no, 1: yes
18	Difficulty preparing a hot meal	0: no, 1: yes
19	Difficulty shopping for groceries	0: no, 1: yes
20	Difficulty making telephone calls	0: no, 1: yes
21	Difficulty taking medications	0: no, 1: yes
22	Difficulty doing work around the house or garden	0: no, 1: yes
23	Difficulty managing money eg paying bills keeping track of expenses	0: no, 1: yes
24	Self-reported general health	0: very good–good, 1: fair–very bad
25	Self-reported eyesight (corrected)	0: excellent-good, 1: fair-poor
26	Self-reported hearing (corrected)	0: excellent-good, 1: fair-poor
27	Chronic: lung disease diagnosis	0: no, 1: yes
28	Chronic: asthma diagnosis	0: no, 1: yes
29	Chronic: arthritis diagnosis	0: no, 1: yes
30	Chronic: osteoporosis diagnosis	0: no, 1: yes
31	Chronic: cancer diagnosis	0: no, 1: yes
32	Chronic: Parkinson’s diagnosis	0: no, 1: yes
33	Chronic: psychiatric condition diagnosis	0: no, 1: yes
34	Chronic: Alzheimer’s diagnosis	0: no, 1: yes
35	Chronic: dementia diagnosis	0: no, 1: yes
36	CVD: high blood pressure diagnosis	0: no, 1: yes
37	CVD: angina diagnosis	0: no, 1: yes
38	CVD: heart attack	0: no, 1: yes
39	CVD: congestive heart failure diagnosis	0: no, 1: yes
40	CVD: heart murmur diagnosis	0: no, 1: yes
41	CVD: abnormal heart rhythm	0: no, 1: yes
42	CVD: diabetes or high blood sugar diagnosis	0: no, 1: yes
43	CVD: stroke diagnosis	0: no, 1: yes

### S1.3 Model selection

We computed the Bayesian Information Criteria (BIC) and out-of-sample (test) log-likelihood across 100 bootstrap replicates. A lower BIC and higher log-likelihood indicate better performing models. In particular, the log-likelihood captures how well the model fits (train) or predicts (test) the specific health trajectories in the data. For each bootstrap iteration, the out-of-sample individuals are those who were not randomly selected, representing approximately  $e^{-1} = 37\%$  of the population. The in-sample are the approximately 63% of individuals who were randomly included. The BIC is computed from the in-sample (train) log-likelihood as

$$\text{BIC} = 6(\text{parameters}) \ln(\text{number of data points}) - 2(\text{in-sample log-likelihood}). \quad (\text{S8})$$

For the survival component, only entries with recorded deaths are included in the number of data points. The log-likelihood is the value of the objective function, Eq. 2.

In Figure S8 we present the BIC and test log-likelihood with bootstrap errors. We find diminishing returns for models more complex than linear in both  $f$  and  $t$ , suggesting it is an efficient model. Note that for the constant model,  $\exp(\gamma_0)$  we included a Gompertz term for the survival hazard ( $\ln(D) = \exp(d_0)$ ,  $\ln(R) = \exp(r_0)$ , and  $\ln(h) = \exp(h_0 + h_t t)$ ), since it represents our simplest model and we know human survival is Gompertzian. All other models pick the same parametric form for all three: damage, repair and mortality rates.

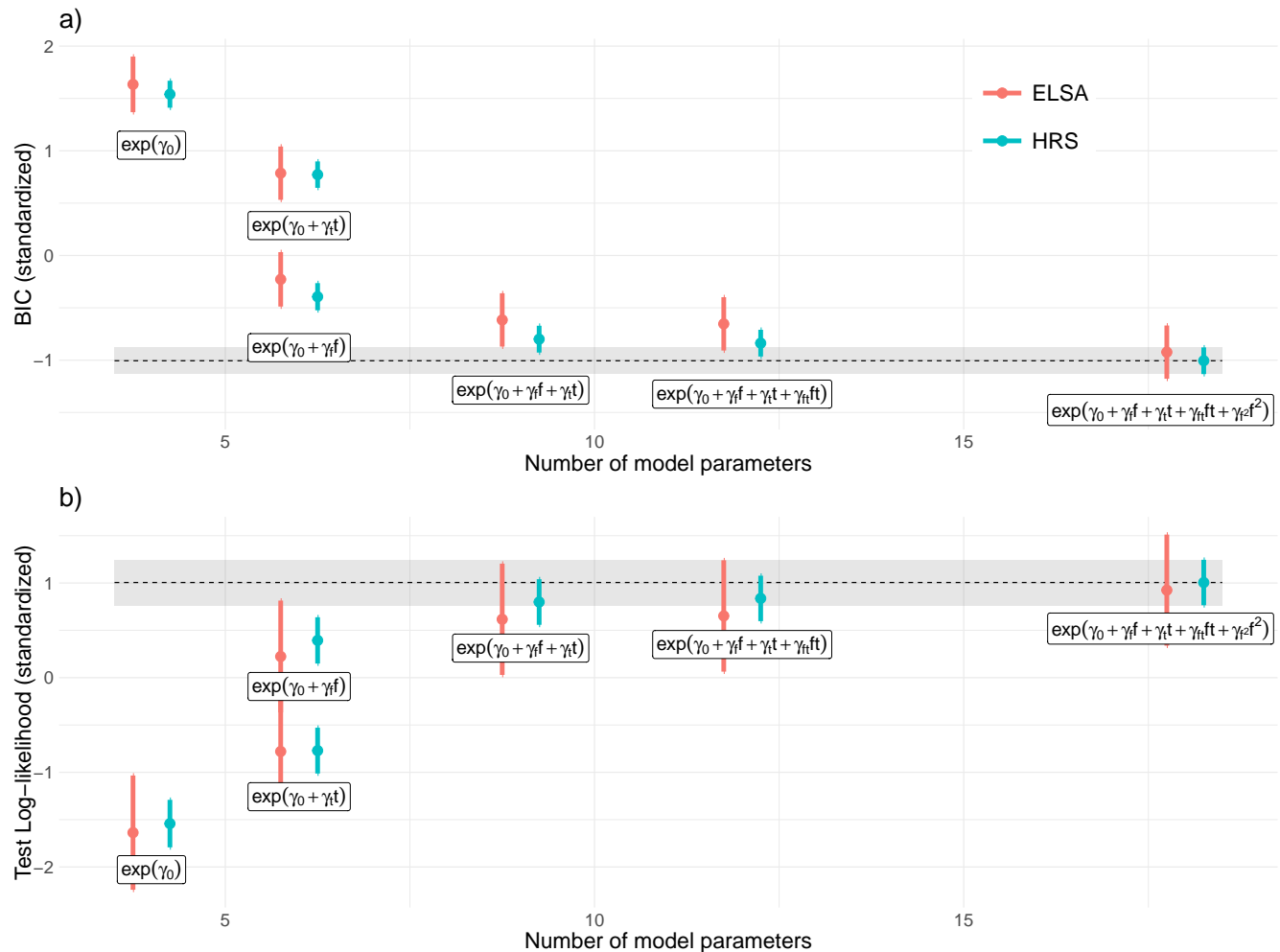


**Figure S8. Conservative model selection** shows that linear terms for both  $f$  and  $t$  are present. More complex models do not appear to improve the fit. Band is best-fitting HRS model. Error bars are standard errors (bootstrap, 100 repeats). Scores have been centered to zero mean and scaled to unit variance for visualization.

Figure S8 may be too conservative since it includes variation in the overall predictability of the population. In Figure S9 we consider the *differences* in BIC and test log-likelihood, where we have bootstrapped comparing the same populations between

the different models. That is, we are comparing the models for 100 replicates of the population, always comparing the models after fitting to the same individuals. Again we find diminishing returns for models more complex than linear in both  $f$  and  $t$ , although here we see a small but significant difference between the linear model and more complex models (particularly after including quadratic  $f^2$ ).

Both the conservative and cavalier model selections indicated diminishing returns past the linear model including  $f$  and  $t$ . The conservative model selection shows non-significant improvement for more complex models whereas the cavalier model selection appears to show significant improvements for more complex models. We infer that the linear model is efficient but it may be possible to improve upon it by including additional terms. We selected the linear model since it is simple and performs as well or almost as well as the more complex models.

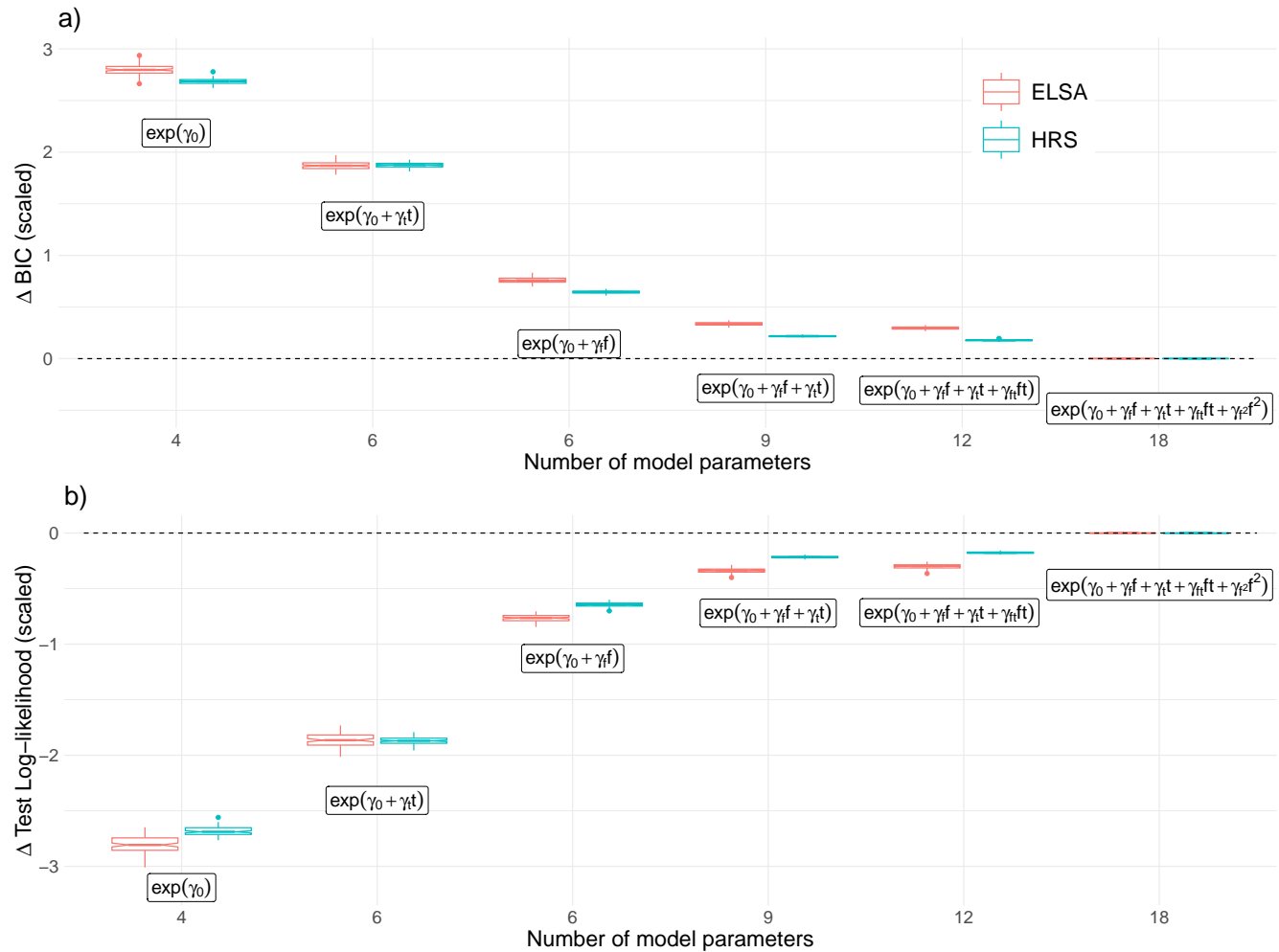


**Figure S9. Cavalier model selection** suggests that additional terms may be present, but there is diminishing returns past the linear,  $\exp(\gamma_0 + \gamma_f f + \gamma_t t)$  model. Boxes are median and interquartile range from scores from bootstrap replicates (100 repeats). Scores have been scaled to unit variance for visualization. Bar is median, notch is approximate 95% CI for median, box is interquartile range (IQR), whiskers are  $1.5 \times \text{IQR}$  or furthest datum<sup>45</sup>.

#### S1.4 Fit diagnostics

In the main text we demonstrate our model recapitulates population-level statistics for a representative sample of models. In Figures S10 (HRS) and S11 (ELSA) we extend the set of models compared. It is interesting that the full Gompertz model,  $\exp(\gamma_0 + \gamma_t t)$ , recapitulates the phenomena despite having a much lower log-likelihood (Section S1.3). This indicates that the time dependence correctly captures the population behaviour but not individual trajectories, which clearly depend on individual health via  $f$ . We note that consistent with Section S1.3, we see that inclusion of an  $f \cdot t$  interaction term does little to modify the model behaviour.

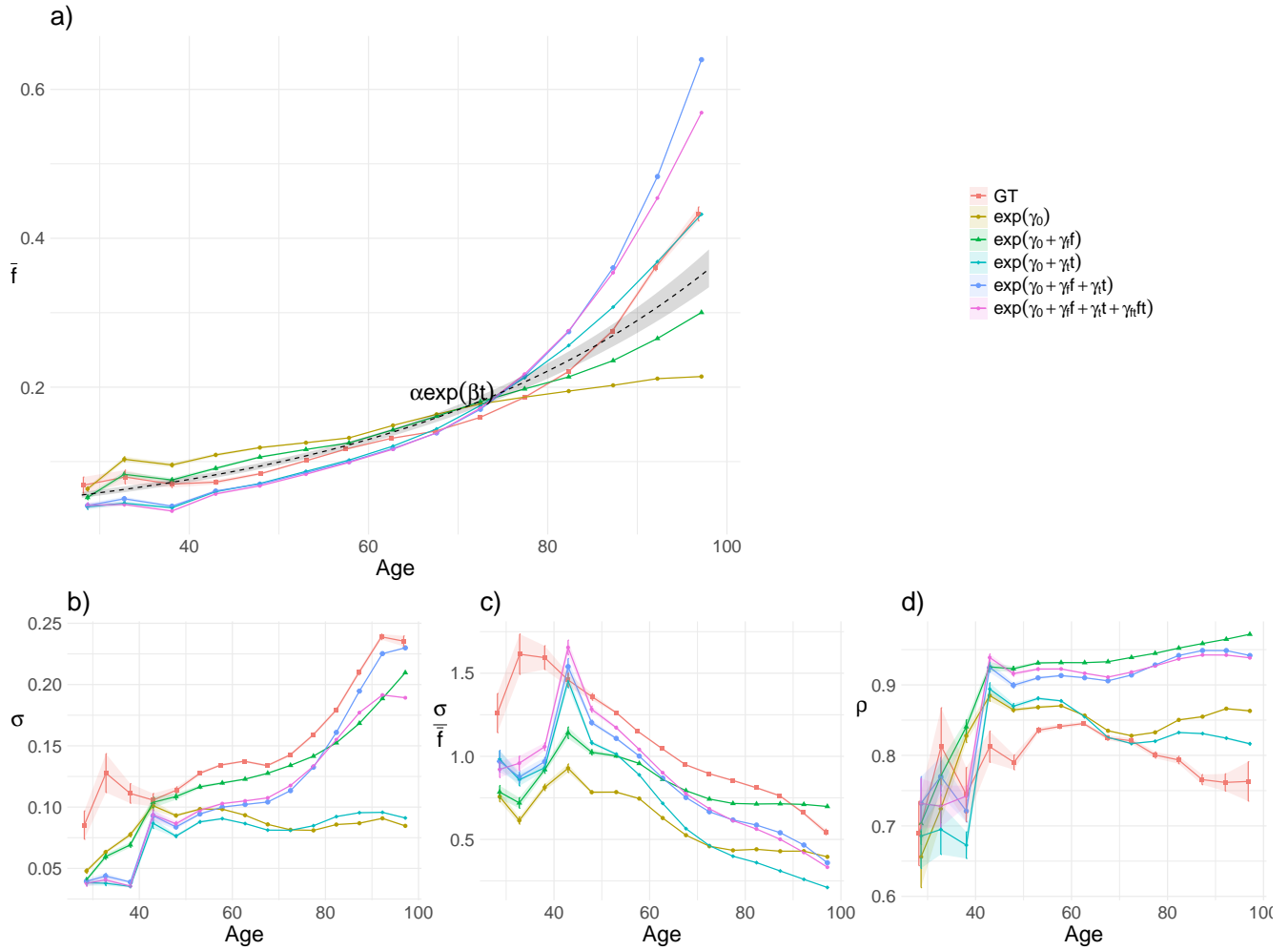


**Figure S10. FI population-level statistics for more models (HRS).** Ground truth (GT) versus simulations using model fits. (a) mean FI,  $\bar{f}$ , (b) FI standard deviation,  $\sigma$ , (c), coefficient of variation  $\sigma/\bar{f}$ , and (d) FI auto-correlation,  $\rho$  (lag-1). Error bars are standard errors (bootstrap, 100 repeats).

Our survival model fit the data reasonably well as visualized in Figure S12. The overall population-level survival was correctly reproduced by the simulation (a), and the (linear) proportional hazard assumption for the FI visually fits reasonably well (b). Note that ELSA survival used end-of-life files which are available for only a subset of individuals, resulting in a much lower mortality rate<sup>24</sup>. As demonstrated by Figures S5 and S7, the age and FI dependence of mortality in both HRS and ELSA were nevertheless similar, with the primary difference being the baseline hazard (much lower for ELSA) and age-dependence (stronger for ELSA). This suggests most of the exclusions in ELSA survival were completely at random, and that our primary results remain consistent between the two studies.

### S1.5 Tuning the effective number of health attributes

The effective number of health attributes depends on the underlying correlation structure, which prior research indicates contains nested domains<sup>16</sup>. This reduces the effective number of deficits compared to our model, which assumes conditional independence given  $f$  and age (which should be sensitive to overall health but not domains). When we simulate fewer deficits we see better quantitative agreement for the higher order statistics, Figure S13. This comes at the cost of the mean, however, which underestimates the curvature at old ages. A plausible reason for this is that the increased variance also increase the hazard<sup>27</sup>, magnifying the survival misfit (Figure S12b). Alternatively, the missing nested correlation structure could be excluding mutual events at older ages. Regardless, our model with fewer effective parameters nevertheless approximates the data reasonably well.

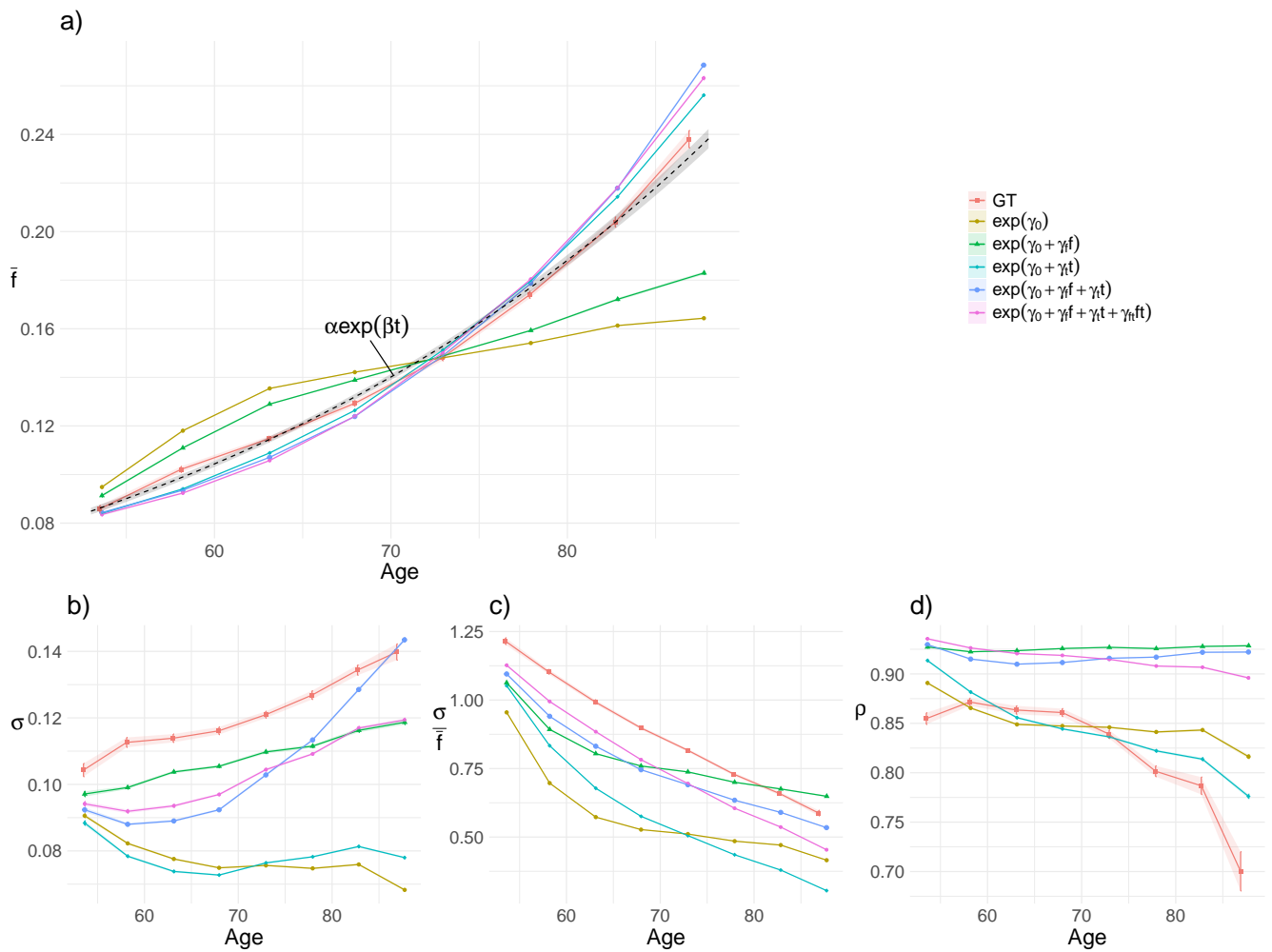


**Figure S11. FI population-level statistics for ELSA.** Ground truth (GT) versus simulations using model fits. (a) mean FI,  $\bar{f}$ , (b) FI standard deviation,  $\sigma$ , (c), coefficient of variation  $\sigma/\bar{f}$ , and (d) FI auto-correlation,  $\rho$  (lag-1). Error bars are standard errors (bootstrap, 100 repeats).

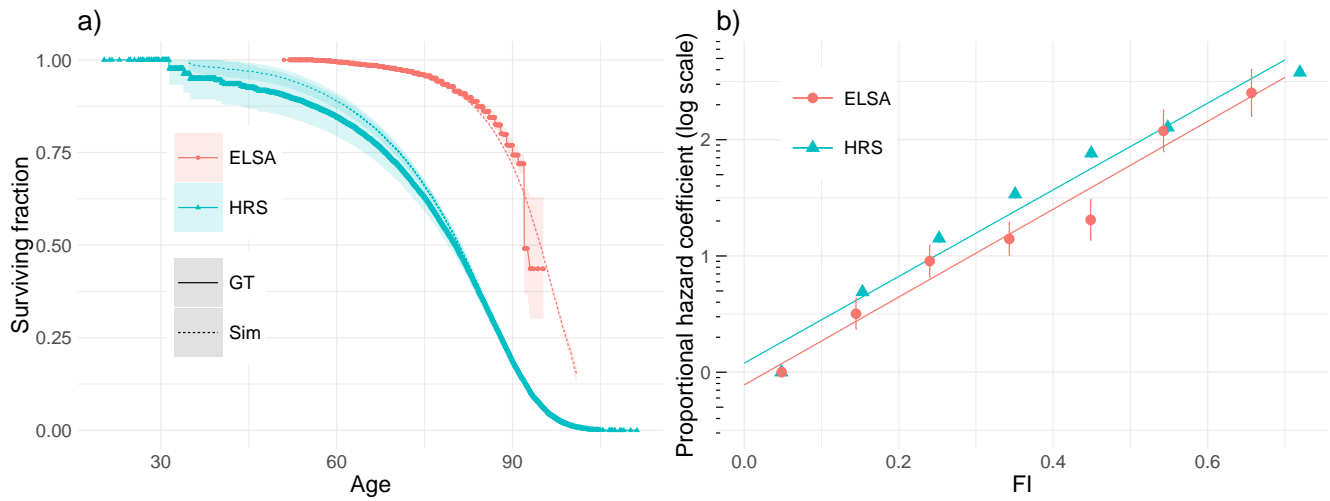


**Figure S12. Survival fit visually well.** (a) Survival simulation visually reproduced the ground truth (GT). (b) linear proportional hazard (lines) approximates the non-parametric hazard (points) well (time-dependent Cox modelling). The model (a) and assumption (b) both fit visually well. HRS appears to be sublinear in  $f$ , however (b). Error bars are standard errors. ELSA has lower mortality due to limited data as discussed in the text.

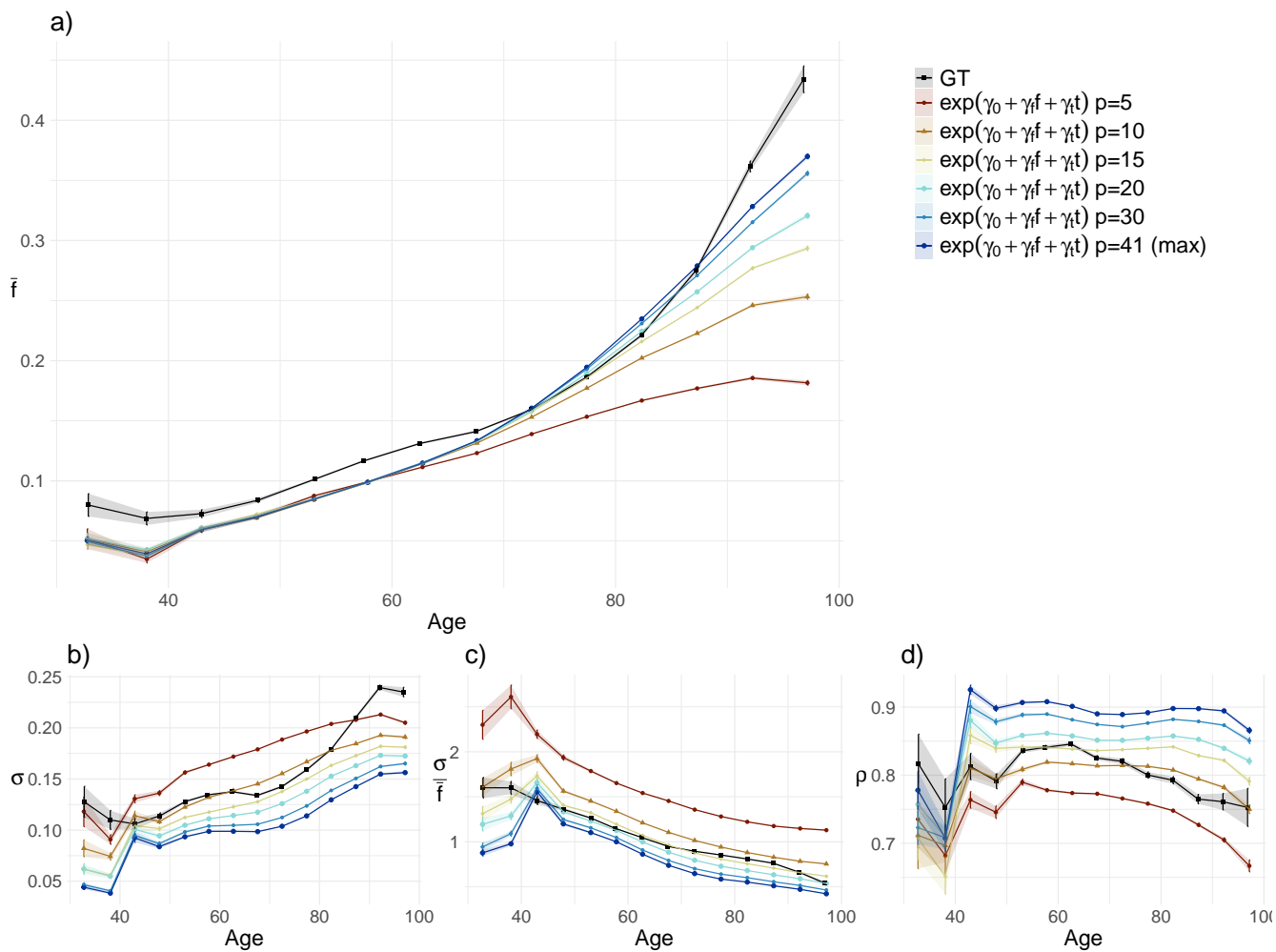


**Figure S13. Number of health attributes strongly affects higher-order statistics**, including standard deviation (b), CV (c) and auto-correlation (d). HRS. We see good visual agreement for these statistics for between 10 (orange triangles) and 20 (teal dots) health attributes rather than the true number, 41. This is likely due to the underlying correlations between health attributes that reduces the degrees of freedom and thus effective number of independent health attributes. The mean appears to fit worse with decreasing number of attributes, however (a). Error bars are standard errors (bootstrap, 100 repeats).

### S1.6 Sex effects

We observed sex differences in the parameter estimates across HRS and ELSA (Figures S14 and S15, respectively). Each point in the boxplot is a bootstrap replicate, meaning that non-overlapping box notches have significantly different median parameter estimates. Males showed lower baseline damage rate  $d_0$  but faster loss of robustness with worsening health  $d_f$  and increasing age  $d_r$ . They also showed a greater loss of resilience with worsening health  $r_f$ , a higher baseline hazard  $h_0$  and a higher hazard due to worse health  $h_f$ . The net cumulative effects of these parameterizations for males is: lower  $\Delta_0$ , higher  $\Delta_f$ , and higher  $\Delta_r$ .

The effect of the parameterization on the nullcline is shown in Figure S16. Males are stable at a lower FI at young ages but a higher FI at older ages. Males are known to have a lower FI than females but do not live as long<sup>40</sup>. According to our parameter estimates this is because males have lower initial damage rate,  $d_0$ , but are more sensitive to loss of robustness and resilience with both age and worsening health,  $\Delta_f$  and  $\Delta_r$ . Death appears to be via higher baseline hazard  $h_0$  and greater sensitivity to poor health  $h_f$ . These results are consistent with males reaching adulthood in a more robust state but being less tolerant to age-related decline. Males appear to age faster but from a better starting point.

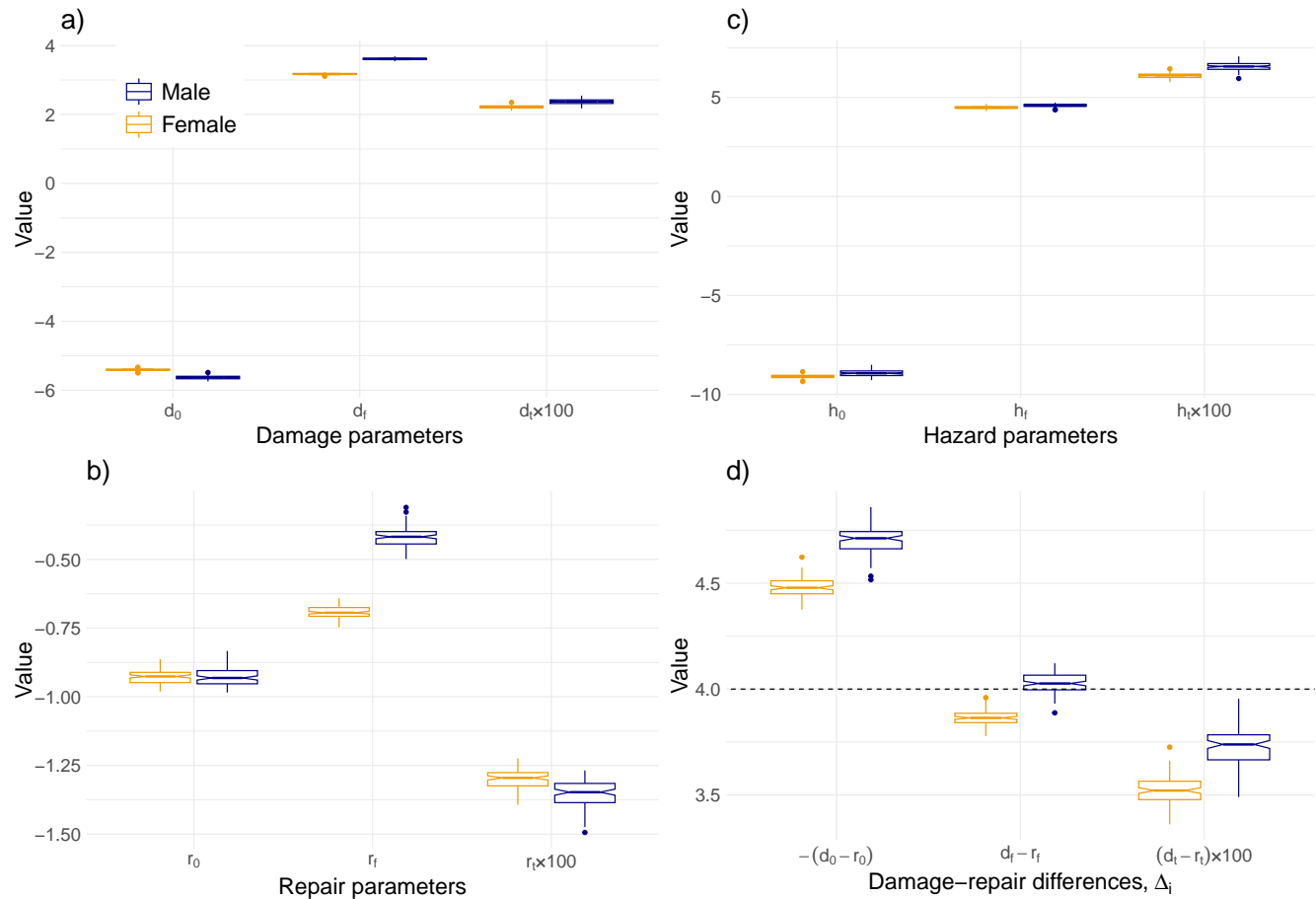


**Figure S14. Parameter estimates by sex – HRS.** Each point is an estimate from 100 bootstrap replicates. Males have better baseline health  $\Delta_0$ , but are more sensitive to poor health  $\Delta_f$  and old ages  $\Delta_r$  (note the signs in d). Bar is median, notch is approximate 95% CI for median, box is interquartile range (IQR), whiskers are  $1.5 \times \text{IQR}$  or furthest datum<sup>45</sup>.



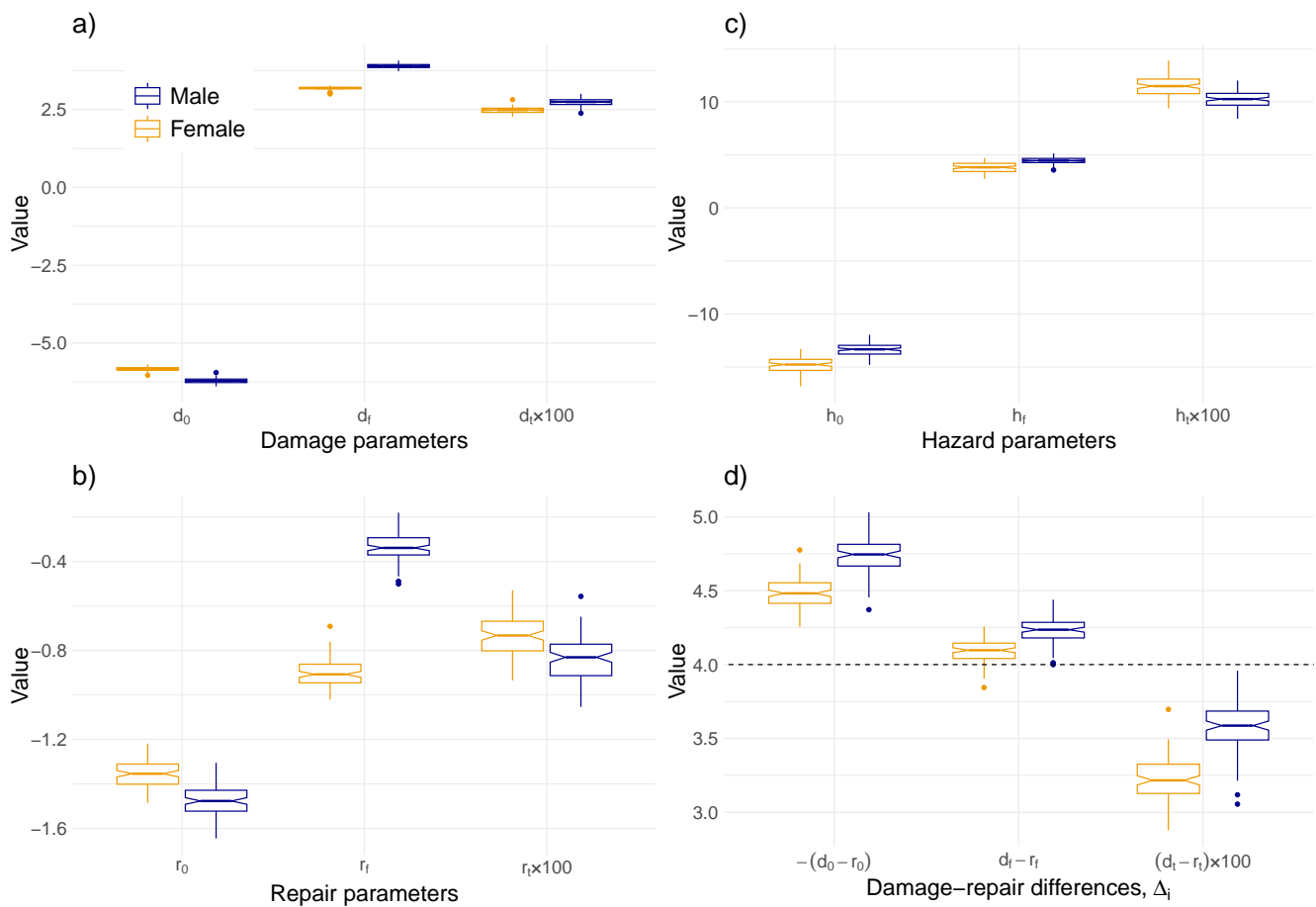


**Figure S15. Parameter estimates by sex – ELSA.** Each point is an estimate from 100 bootstrap replicates. As with HRS, males have better baseline health  $\Delta_0$ , but are more sensitive to poor health  $\Delta_f$  and old ages  $\Delta_r$  (note the signs in d). Bar is median, notch is approximate 95% CI for median, box is interquartile range (IQR), whiskers are  $1.5 \times \text{IQR}$  or furthest datum<sup>45</sup>.

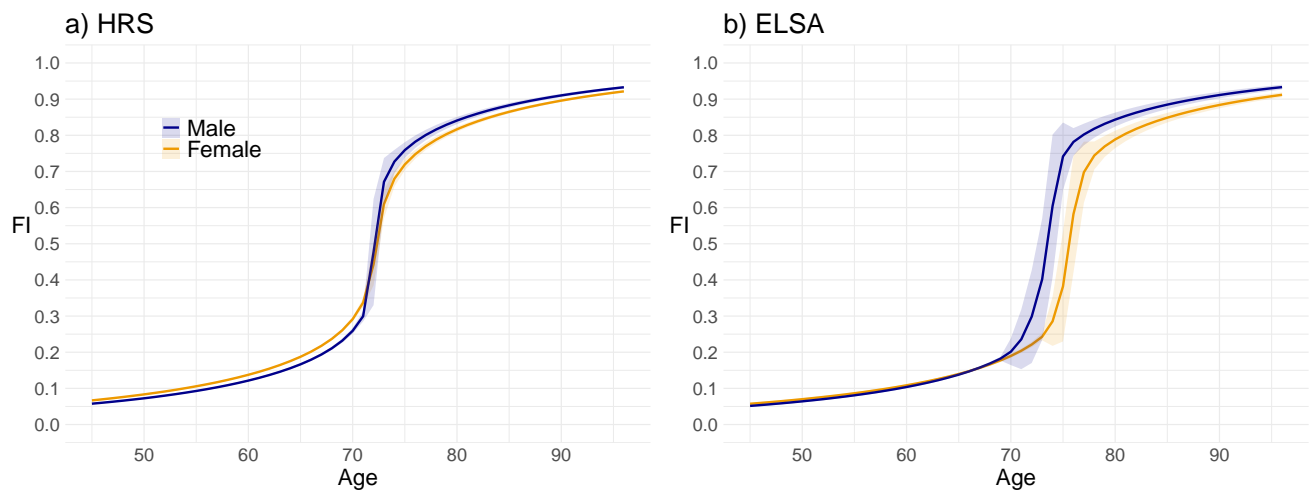


**Figure S16. Nullcline by sex based on parameter values.** Males consistently start out lower at young ages but cross and end up higher at older ages. Error bars are standard errors (bootstrap, 100 repeats).

### S1.7 Nullcline analysis

Figure 4 demonstrates that for our parameter values there is a tipping point near age 75. Here we analytically show that this occurs for  $\Delta_f = 4$ , consistent with model estimates from the data.

Take the FI dynamics of our best model are (Section S1.3),

$$\frac{d}{dt}f = (1-f)\exp\left(d_0 + d_f f + d_t t\right) - f\exp\left(r_0 + r_f f + r_t t\right) \quad (\text{S9})$$

where  $f$  is the FI.

From here there are five key steps: (i) find the nullcline where  $df/dt = 0$ , (ii) solve for  $t^*(f^*)$ , (iii) find the critical points of  $t^*(f^*)$ , (iv) solve for  $\Delta_f(f) \equiv d_f - r_f$ , and finally (v) find the critical points  $\Delta_f^*(f)$ . The nullcline occurs when the derivative is 0 i.e.

$$\ln(1-f^*) + d_0 + d_f f^* + d_t t^* = \ln(f^*) + r_0 + r_f f^* + r_t t^*. \quad (\text{S10})$$

It is useful to define

$$\Delta_i \equiv d_i - r_i, \quad (\text{S11})$$

then we rearrange and solve for  $t$ ,

$$\begin{aligned} t^* \Delta_t &= -\Delta_0 - \Delta_f f^* + \ln\left(\frac{f^*}{1-f^*}\right) \\ \implies t^* &= -\frac{\Delta_0}{\Delta_t} - \frac{\Delta_f}{\Delta_t} f^* + \frac{1}{\Delta_t} \ln\left(\frac{f^*}{1-f^*}\right). \end{aligned} \quad (\text{S12})$$

This defines a curve, though not necessarily a function (since more than one value of  $f^*$  could have the same  $t^*$ ). This curve has a discontinuity when  $dt^*/df^* = 0$ ,

$$\begin{aligned} \frac{dt^*}{df^*} &= \frac{-\Delta_f + \frac{1-f^*}{f^*} \left( \frac{1}{1-f^*} + \frac{f^*}{(1-f^*)^2} \right)}{\Delta_t} \\ &= -\frac{\Delta_f}{\Delta_t} + \frac{1}{\Delta_t f^*(1-f^*)}. \end{aligned} \quad (\text{S13})$$

We can have  $dt^*/df^* = 0$  only if

$$\begin{aligned} \Delta_f &= \frac{1}{f^*(1-f^*)}, \\ \implies f^*(1-f^*) &= \frac{1}{\Delta_f}. \end{aligned} \quad (\text{S14})$$

When can this happen? The critical points of  $x(1-x)$  are

$$\begin{aligned} 1-x^* &= x^*, \\ \implies x^* &= 1/2 \end{aligned} \quad (\text{S15})$$

with  $.5^2 = 1/4$  being the value taken at this point.  $1/4$  is the maximum of  $x(1-x)$ , which is symmetrical about  $x = 1/2$  and bounded by 0.

This means that the smallest possible value of  $\Delta_f$  for which there exists a critical point is  $\Delta_f = 4$ . At the critical point  $dt^*/df^* = 0$  and hence  $df^*/dt^* \rightarrow \infty$  diverges leading to a discontinuity. For larger  $\Delta_f$  the solutions bifurcate; for smaller there is no solution.

We have  $\Delta_f \approx 4$  and hence we know  $\bar{f}^* \approx 1/2$ . For  $\bar{f}^* = 1/2$  the critical time,  $t^*$ , has a discontinuity at  $72.3 \pm 0.3$  years for HRS and  $75.0 \pm 0.5$  years for ELSA, consistent with what was observed in Figures 2 and 3. Note that for  $\Delta_f = 4$  the expression is simply  $t^* = -\Delta_0/\Delta_t - 2/\Delta_t$ .

### S1.8 Objective function

We fit to longitudinal health deficit data and survival using the modified log-likelihood including survival and its gradient, then optimizing using the BFGS quasi-Newton's method<sup>25</sup>. The fit is repeated 100 times via bootstrapping i.e. random sampling of individuals from the population (with replacement). The log-likelihood is based on transition rates between states, and is shown to be consistent with the stochastic model of the FI, Eq. 1, in Section S1.8.2.

We consider the survival-modified likelihood using the *a posteriori*

$$\begin{aligned} p(\text{data}|\text{parameters}) &= p(\text{parameters}|\text{data})p(\text{data}) \\ &= \text{likelihood} \cdot \text{prior}. \end{aligned} \quad (\text{S16})$$

We know that  $p(\text{data})$  is 0 if an individual is dead and should gradually decrease from 1 to 0 as an individual's health declines. We can measure this decline by the FI and hence

$$p(\text{data}|f, \Delta t, \delta) = S(f, \Delta t)h(f, \Delta t)^\delta \quad (\text{S17})$$

where  $S$  is the probability of surviving from the previous measurement to the current time point,  $\delta = 1$  if the individual is dead and 0 otherwise. The observation of each datum will have this term.

We can then write the survival-modified likelihood as

$$p = \prod_{i=1}^N \prod_{j=1}^p \prod_{k=1}^{T-1} \left[ \text{Pr}(b_{ijk} = 1 | b_{ik-1}, f_{ik-1})^{b_{ijk}} (1 - \text{Pr}(b_{ijk} = 1 | b_{ik-1}, f_{ik-1}))^{1-b_{ijk}} \right]^{1-\delta_{ik}} S(f_{ik}, f_{ik-1}, \Delta t_{ik}) h(f_{ik}, f_{ik-1})^{\delta_{ik}}. \quad (\text{S18})$$

On the log scale,

$$\begin{aligned} l &= \sum_{i=1}^N \sum_{j=1}^p \sum_{k=1}^{T-1} (1 - \delta_{ik}) \left[ b_{ijk} \ln(\text{Pr}(b_{ijk} = 1 | b_{ik-1}, f_{ik-1})) + (1 - b_{ijk}) \ln(1 - \text{Pr}(b_{ijk} = 1 | b_{ik-1}, f_{ik-1})) \right] \\ &+ \sum_{i=1}^N \sum_{k=1}^{T-1} \left[ \ln(S(f_{ik}, f_{ik-1}, \Delta t_{ik})) + \delta_{ik} \ln(h(f_{ik}, f_{ik-1})) \right]. \end{aligned} \quad (\text{S19})$$

where we have  $N$  individuals,  $p$  variables and  $T$  time points. The first term captures health transitions and the second captures survival.

The likelihood has four cases for health transitions:

$$1 - S_d \approx \text{Pr}(b_{ik-1} = 0 \text{ and } b_{ik} = 1) \text{ (damage)}, \quad (\text{S20a})$$

$$1 - S_r \approx \text{Pr}(b_{ik-1} = 1 \text{ and } b_{ik} = 0) \text{ (repair)}, \quad (\text{S20b})$$

$$S_r \approx \text{Pr}(b_{ik-1} = 1 \text{ and } b_{ik} = 1) \text{ ('survived' repair)}, \quad (\text{S20c})$$

$$S_d \approx \text{Pr}(b_{ik-1} = 0 \text{ and } b_{ik} = 0) \text{ ('survived' damage)}, \quad (\text{S20d})$$

where  $S_d$  and  $S_r$  are defined as the survival probability for damage and repair, respectively. Specifically,

$$S_d \equiv \exp\left(-\int_{t_{k-1}}^{t_k} D(f, t) dt\right) \quad (\text{S21a})$$

$$S_r \equiv \exp\left(-\int_{t_{k-1}}^{t_k} R(f, t) dt\right) \quad (\text{S21b})$$

where  $D$  and  $R$  are the damage and repair hazards, respectively.

There are an infinite number of paths connecting each time point pair, and in principle variables may have an infinite number of damage/repair cycles between measurements. These cycles are regulated by  $\Delta t$  e.g.

$$\begin{aligned} \text{Pr}(b_{ik-1} = 0 \text{ and } b_{ik} = 0) &= S_d + (1 - S_d)(1 - S_r) + \dots \\ &\approx 1 - D\Delta t + DR\Delta t^2 + O(\Delta t^3) \\ &\approx S_d. \end{aligned} \quad (\text{S22})$$

In general, the lowest order ( $\Delta t$ ) for each of the four cases is given by  $S_r$ ,  $S_d$ ,  $1 - S_r$  or  $1 - S_d$ . Thus for sufficiently small  $\Delta t$  we can concern ourselves entirely with the survival probabilities.

The likelihood in terms of  $S_r$  and  $S_d$  is thus

$$\begin{aligned}
l \equiv & \sum_{i=1}^N \sum_{j=1}^p \sum_{k=1}^{T-1} (1 - \delta_{ik}) \left[ \right. \\
& b_{ijk}(1 - b_{ijk-1}) \ln(1 - S_d) \\
& + (1 - b_{ijk})b_{ijk-1} \ln(1 - S_r) \\
& + b_{ijk}b_{ijk-1} \ln(S_r) \\
& \left. + (1 - b_{ijk})(1 - b_{ijk-1}) \ln(S_d) \right] \\
& + \sum_{i=1}^N \sum_{k=1}^{T-1} \left[ \ln(S(f_{ik}, f_{ik-1}, \Delta t_{ik})) + \delta_{ik} \ln(h(f_{ik}, f_{ik-1})) \right], \tag{S23}
\end{aligned}$$

which becomes exact in the small  $\Delta t$  limit (small enough that multiple events between time points becomes negligible).

### S1.8.1 Gradient

The gradient is needed for efficient optimization. Assume that the model parameters for  $D$  are  $\vec{\theta}_d$ ,  $R$  are  $\vec{\theta}_r$ , and  $h$  are  $\vec{\theta}_h$  with no overlap between the three. The gradient in general form is then

$$\begin{aligned}
\frac{\partial}{\partial \theta_{dn}} l = & \sum_{i=1}^N \sum_{j=1}^p \sum_{k=1}^{T-1} (1 - \delta_{ik}) \left[ \right. \\
& b_{ijk}(1 - b_{ijk-1}) \frac{-S_d}{(1 - S_d)} \left( - \int_{t_{k-1}}^{t_k} \frac{\partial}{\partial \theta_{dn}} D(f, t) dt \right) \\
& \left. + (1 - b_{ijk})(1 - b_{ijk-1}) \left( - \int_{t_{k-1}}^{t_k} \frac{\partial}{\partial \theta_{dn}} D(f, t) dt \right) \right], \tag{S24a}
\end{aligned}$$

$$\begin{aligned}
\frac{\partial}{\partial \theta_{rn}} l = & \sum_{i=1}^N \sum_{j=1}^p \sum_{k=1}^{T-1} (1 - \delta_{ik}) \left[ \right. \\
& + (1 - b_{ijk})b_{ijk-1} \frac{-S_r}{(1 - S_r)} \left( - \int_{t_{k-1}}^{t_k} \frac{\partial}{\partial \theta_{rn}} R(f, t) dt \right) \\
& \left. + b_{ijk}b_{ijk-1} \left( - \int_{t_{k-1}}^{t_k} \frac{\partial}{\partial \theta_{rn}} R(f, t) dt \right) \right], \text{ and} \tag{S24b}
\end{aligned}$$

$$\frac{\partial}{\partial \theta_{hn}} l = \sum_{i=1}^N \sum_{k=1}^{T-1} \left( - \int_{t_{k-1}}^{t_k} \frac{\partial}{\partial \theta_{hn}} h(f, t) dt \right) + \delta_{ik} \frac{1}{(h(f_{ik}, f_{ik-1}))} \left( \frac{\partial}{\partial \theta_{hn}} h(f, t) \right). \tag{S24c}$$

### Rate Models

An important consideration for the hazards is non-negativity, which is preferably hard-coded by choice of model. The most general but solvable exponential model is a generalized additive model with Gompertz term,

$$D(f, t) \equiv \exp \left( \sum_j d_j \phi_j(f) + t \sum_j d_{tj} \phi_j(f) \right), \tag{S25a}$$

$$R(f, t) \equiv \exp \left( \sum_j r_j \phi_j(f) + t \sum_j r_{tj} \phi_j(f) \right), \text{ and} \tag{S25b}$$

$$h(f, t) \equiv \exp \left( \sum_j h_j \phi_j(f) + t \sum_j h_{tj} \phi_j(f) \right), \tag{S25c}$$

where  $\phi_j(f)$  is any desired function of  $f$ , for our purposes we use a constant (1) or polynomial. The derivatives are

$$\frac{\partial}{\partial d_n} D(f, t) = D(f, t) \phi_n(f), \quad (\text{S26a})$$

$$\frac{\partial}{\partial d_{tn}} D(f, t) = t D(f, t) \phi_n(f), \quad (\text{S26b})$$

$$\frac{\partial}{\partial r_n} R(f, t) = R(f, t) \phi_n(f), \quad (\text{S26c})$$

$$\frac{\partial}{\partial r_{tn}} R(f, t) = t R(f, t) \phi_n(f), \quad (\text{S26d})$$

$$\frac{\partial}{\partial h_n} h(f, t) = h(f, t) \phi_n(f). \quad (\text{S26e})$$

$$\frac{\partial}{\partial h_{tn}} h(f, t) = t h(f, t) \phi_n(f). \quad (\text{S26f})$$

The gradient (Eq. S24c) depends on the integral of these over a time interval, which are

$$- \int_{t_{k-1}}^{t_k} \frac{\partial}{\partial \alpha_d} D(f, t) dt = \frac{1}{\alpha_d^2} D(f, t_{k-1}) (\alpha_d t_{k-1} - 1 + (1 - \alpha_d t_k) \exp(\alpha_d \Delta t)), \quad (\text{S27a})$$

$$- \int_{t_{k-1}}^{t_k} \frac{\partial}{\partial d_n} D(f, t) dt = \frac{1}{\alpha_d} D(f, t_{k-1}) (1 - \exp(\alpha_d \Delta t)) \phi_n(f), \quad (\text{S27b})$$

$$- \int_{t_{k-1}}^{t_k} \frac{\partial}{\partial \alpha_r} R(f, t) dt = \frac{1}{\alpha_r^2} R(f, t_{k-1}) (\alpha_r t_{k-1} - 1 + (1 - \alpha_r t_k) \exp(\alpha_r \Delta t)), \quad (\text{S27c})$$

$$- \int_{t_{k-1}}^{t_k} \frac{\partial}{\partial r_n} R(f, t) dt = \frac{1}{\alpha_r} R(f, t_{k-1}) (1 - \exp(\alpha_r \Delta t)) \phi_n(f), \quad (\text{S27d})$$

$$- \int_{t_{k-1}}^{t_k} \frac{\partial}{\partial \alpha_h} h(f, t) dt = \frac{1}{\alpha_h^2} h(f, t_{k-1}) (\alpha_h t_{k-1} - 1 + (1 - \alpha_h t_k) \exp(\alpha_h \Delta t)), \text{ and} \quad (\text{S27e})$$

$$- \int_{t_{k-1}}^{t_k} \frac{\partial}{\partial h_n} h(f, t) dt = \frac{1}{\alpha_h} h(f, t_{k-1}) (1 - \exp(\alpha_h \Delta t)) \phi_n(f). \quad (\text{S27f})$$

Where

$$\alpha_d \equiv \sum_j d_{tj} \phi_j(f), \quad (\text{S28a})$$

$$\alpha_r \equiv \sum_j r_{tj} \phi_j(f), \text{ and} \quad (\text{S28b})$$

$$\alpha_h \equiv \sum_j h_{tj} \phi_j(f). \quad (\text{S28c})$$

If we wish to take the Gompertz term  $\alpha \rightarrow 0$  we can simply substitute  $(1 - e^{\alpha\Delta t})/\alpha \rightarrow -\Delta t$ .

We can then use chain rule to get the derivatives in terms of model parameters,

$$\frac{\partial \alpha_d}{\partial d_{in}} = \phi_n, \quad (\text{S29a})$$

$$\frac{\partial \alpha_r}{\partial r_{in}} = \phi_n, \text{ and} \quad (\text{S29b})$$

$$\frac{\partial \alpha_h}{\partial h_{in}} = \phi_n, \quad (\text{S29c})$$

hence we simply multiply by  $\phi_n$ .

### S1.8.2 The objective function is well-posed

Our derived model is a stochastic model of  $f$ , Eq. 1. To fit the model to the data we derived a likelihood function based on transition rates. Here we show that in the mean field approximation we recover Eq. 1 and hence the objective function is well-posed.

Assuming transition rate models for damage,  $D(f, t)$ , and repair,  $R(f, t)$ , the probability of observing  $p_d$  deficits in  $p$  attributes is a Markov model of the form

$$\begin{aligned} Pr(p_d(t + \Delta t) | p_d(t)) &= \sum_{r=0}^{p_d(t)} Pr(r \text{ repairs}) Pr(d \text{ damage}) \\ &= \sum_{r=0}^{p_d(t)} \binom{p_d(t)}{r} (1 - S_r)^r (S_r)^{p_d(t)-r} \binom{p - p_d(t)}{d} (1 - S_d)^d (S_d)^{p - p_d(t) - d} \end{aligned} \quad (\text{S30})$$

where  $d = p_d(t + \Delta t) - p_d(t) + r = \Delta p_d + r$  is constrained. Also note that  $S_r$  is the probability of not repairing and  $S_d$  is the probability of not damaging during the time step  $\Delta t$ .

If we take the limit  $\Delta t \rightarrow 0$  we find

$$Pr(p_d(t + dt) | p_d(t)) = \begin{cases} 1 - p_d(t)R(f, t)dt - (p - p_d(t))D(f, t)dt & \text{if } \Delta p = 0 \\ p_d(t)R(f, t)dt & \text{if } \Delta p = -1 \\ (p - p_d(t))D(f, t)dt & \text{if } \Delta p = 1 \\ 0 & \text{if } |\Delta p| > 1 \end{cases} \quad (\text{S31})$$

where all  $\mathcal{O}(dt^2) \rightarrow 0$  (and higher powers). Keep in mind that  $p_d(t) = pf(t)$  (by definition of  $f$ ) and  $0 \leq p_d(t + dt) \leq p$  will constrain certain values. Note that due to the general rule for marginalizing,  $Pr(p_d(t + dt)) = \langle Pr(p_d(t + dt) | p_d(t)) \rangle_{p_d(t)}$ , thus we can use Eq. S31 to find the marginal average using  $\langle \langle p_d(t + dt) \rangle_{p_d(t)} \rangle_{p_d(t)}$  (i.e. average first over  $Pr(p_d(t + dt) | p_d(t))$  then over  $p_d(t)$ ). To be clear,  $\langle x \rangle_y$  denotes averaging  $x$  over all possible  $y$ .

Since the FI is defined by  $p_d/p$ , for constant  $p$ , we can use Eq S31 to compute the average FI, this yields the differential equation

$$\frac{d}{dt} \bar{f} = \langle (1 - f)D(f) \rangle - \langle fR(f) \rangle \quad (\text{S32})$$

which to mean-field approximation (zeroth order) is

$$\frac{d}{dt} \bar{f} \approx (1 - \bar{f})D(\bar{f}, t) - \bar{f}R(\bar{f}, t) \quad (\text{S33})$$

which is exact when  $\phi_i(f) \equiv 1$  i.e.  $D$  and  $R$  are constant;  $\bar{f} \equiv \langle f \rangle$ . Observe that this is exactly Eq. 1 with substitution  $f \rightarrow \bar{f}$ .

The next highest order includes additional terms,

$$\frac{d}{dt} \bar{f} \approx \left[ 1 - \bar{f} - \sum_i d_i \frac{d\phi_i(\bar{f})}{df} \text{Var}(f) \right] D(\bar{f}, t) - \left[ \bar{f} + \sum_i r_i \frac{d\phi_i(\bar{f})}{df} \text{Var}(f) \right] R(\bar{f}, t). \quad (\text{S34})$$

For sufficiently large number of attributes, the variance term will become small relative to the mean and we can ignore the higher-order corrections. Hence our objective function is well-posed as it approximates our desired dynamical equation.

## S1.9 Stability analysis

We can summarize the approximate behaviour of the model by assuming small  $f$  (relative to both  $d_f$  and  $r_f$ ). This permits us to better compare our results to other researchers'. The approximation is justified by the observed small parameter values (Figure S7), the small nullcline at young ages (Figure 4), and the population-level density that shows most individuals are measured at small  $f$  (Figure S6) – all of these are evidence that the data are predominantly of low  $f$  individuals.

Eq. 1 with the selected model is

$$\begin{aligned} \frac{df}{dt} &= (1-f)e^{d_0+d_f f+d_f t} - f e^{r_0+r_f f+r_f t} \\ &\approx e^{d_0+d_f t} - (e^{r_0+r_f t} + e^{d_0+d_f t} - d_f e^{d_0+d_f t})f \end{aligned} \quad (\text{S35})$$

to linear order in  $f$ . Thus the general form is

$$\frac{df}{dt} = \gamma(t) + \alpha(t)f \quad (\text{S36})$$

for small  $f$ .  $\gamma(t)$  represents unmitigated damage, which increases with age, and  $\alpha(t)$  captures the stability of the feedback and also increases with age. For  $\alpha(t) < 0$  the system is stable and  $f$  will tend to recover from perturbations that increase it. We expect a homeostatic system to be stable and thus have  $\alpha(t) < 0$ , which we have previously observed consistently using a different analysis<sup>46</sup>. For  $\alpha(t) > 0$  the system is unstable and perturbations that increase  $f$  will compound, driving the system to higher values of  $f$ . At  $\alpha(t) = 0$  the system is marginally-stable and is driven entirely by  $\gamma(t)$ . Importantly, we are able to estimate at which age  $\alpha(t)$  will change sign and therefore stability. For HRS we estimate the age is  $103.6 \pm 0.5$  years-old. These ages are considerably older than our estimates for the tipping point, where the small  $f$  approximation begins to become unrealistic. Nevertheless the approximation still qualitatively captures the behaviour of the full model. Whereas the approximate model becomes unstable, the full model instead saturates at a value close to  $f \approx 1$ .

A loss of stability with age has been recapitulated by other researchers. Avchaciov *et al.* inferred a transition from stable to unstable near the lifespan of mice<sup>42</sup>. Karin *et al.*<sup>41</sup> and subsequent work by that lab<sup>47</sup> inferred a transition from stable damage regulation to saturated damage removal in mice senescent cells and E. coli cell membranes, respectively. All of these works also performed dynamical analysis of aging data and reach a similar conclusion: that there is a stable phase of good health at young ages that ends with an unstable phase near the end of life – consistent with our results.

## S1.10 Simulation

We simulate using inverse-transform sampling (Section S1.10.1). We seed the simulation using the complete case data from the initial wave for each study, including each individual's starting deficits and baseline age. The simulation then generates artificial waves sampled with the same average frequency as the observed data.

### S1.10.1 Inverse-transform sampling

In inverse-transform sampling, a probability density function is exactly sampled by sampling from a uniform distribution on  $(0, 1)$  and then transforming using the associated inverse cumulative probability function. The sampling function is thus (e.g. see<sup>48</sup>),

$$\tau(f, t_k, t_{k-1}) = \frac{1}{\alpha} \ln \left( 1 - \frac{\alpha}{\Gamma(f, t_{k-1})} \ln(u) \right) + t_{k-1}, \text{ where} \quad (\text{S37a})$$

$$u \sim \text{uniform}(0, 1). \quad (\text{S37b})$$

Accept-reject sampling<sup>49</sup> is then used to determine if a death event occurs within the sampling interval  $t_k$  and  $t_{k+1}$ . For  $\alpha < 0$  all samples of  $u < \exp\left(\frac{\Gamma(f, t_{k-1})}{\alpha}\right)$  will give negative  $\exp(\tau) < 0$ , which are discarded assuming no event to preserve the correct distribution.

If  $\alpha \equiv 0$  we have the exponential survival model<sup>48</sup> as a special case

$$\tau(f, t_k, t_{k-1}) = -\frac{\ln(u)}{\Gamma(f, t_{k-1})} + t_{k-1}, \text{ where} \quad (\text{S38a})$$

$$u \sim \text{uniform}(0, 1). \quad (\text{S38b})$$

Damage and repair events were sampled using the survival functions ( $S_d$  and  $S_r$ , Eq. S21). We sampled a random variable from a uniform distribution from 0 to 1,  $u \in [0, 1]$  and recorded an event if the random variable exceeded the respective survival function,  $u_d < S_d$  or  $u_r < S_r$ .

The algorithm proceeds as follows:

- For each individual, initialize set of binary variables each as 0 or 1.
- while  $t < t_{max}$ 
  - Increment  $t_k = t_{k-1} + \Delta t$ .
  - Carry forward all previous values  $\vec{b}(t_{k-1})$  and conditions (alive/dead).
  - For each individual sample  $\tau_h$ . If  $\tau_h < t_{k+1}$  kill that individual and set their time of death at  $\tau_h$ .
  - For each individual and each deficit variable ( $b = 1$ ) sample  $u_r \in [0, 1]$  for repair. If  $u_r > S_r(t_k)$  then repair i.e. set  $b = 0$ .
  - For each individual and each repaired variable ( $b = 0$ ) sample  $u_d \in [0, 1]$  for damage. If  $u_d > S_d(t_k)$  then damage i.e. set  $b = 1$ .

This algorithm is not formally exact since it doesn't permit multiple repair/damage cycles between time steps. However, as discussed in Eq. S22, these cycles are all order  $(\Delta t)^2$  or higher, meaning that if  $\Delta t$  is sufficiently small the algorithm becomes arbitrarily close to the true model.

The lowest-order correction is proportional to  $DR\Delta t^2$  compared to  $1 - D\Delta t$  or  $1 - R\Delta t$  thus the relative error (for small  $\Delta t$ ) for these terms are

$$\text{relative error} = \frac{DR\Delta t^2}{1 - R\Delta t + DR\Delta t^2} \approx DR\Delta t^2, \text{ and} \quad (\text{S39a})$$

$$\text{relative error} = \frac{DR\Delta t^2}{1 - D\Delta t + DR\Delta t^2} \approx DR\Delta t^2. \quad (\text{S39b})$$

E.g. if  $DR\Delta t^2 = 0.01$  then the algorithm has approximately a 1% relative error for damage and repair effects (specifically  $b(t_{k-1}) = 0 \rightarrow b(t_k) = 0$  and  $b(t_{k-1}) = 1 \rightarrow b(t_k) = 1$  transitions).  $D$  and  $R$  are typically small,  $\ll 1$  (Figure S5). We found that  $\Delta t = 0.2$  years is small enough that the simulation no longer depends on the step size (not shown). We thus simulated at  $\Delta t = 0.2$  years and saved every approximately 10 iterations to produce simulated waves that emulate the observed data.